Journal of Oceanography, Vol. 61, pp. 921 to 942, 2005

An Ecosystem Model Including Nitrogen Isotopes: Perspectives on a Study of the Marine Nitrogen Cycle

CHISATO YOSHIKAWA[1]*, YASUHIRO YAMANAKA[1,2] and TAKESHI NAKATSUKA[3]

[1]*Graduate School of Environmental Earth Science, Hokkaido University, Kita-ku, Sapporo 060-0810, Japan*
[2]*Frontier Research Center for Global Change, Japan Agency for Marine-Earth Science and Technology, Showamachi, Kanazawa-ku, Yokohama 236-0001, Japan*
[3]*Institute of Low Temperature Science, Hokkaido University, Kita-ku, Sapporo 060-0819, Japan*

(Received 15 September 2004; in revised form 21 February 2005; accepted 6 March 2005)

We have developed an ecosystem model including two nitrogen isotopes (^{14}N and ^{15}N), and validated this model using an actual data set. A study of nitrogen isotopic ratios (δ^{15}N) using a marine ecosystem model is thought to be most helpful in quantitatively understanding the marine nitrogen cycle. Moreover, the model study may indicate a new potential of δ^{15}N as a tracer. This model has six compartments: phytoplankton, zooplankton, particulate organic nitrogen, dissolved organic nitrogen, nitrate and ammonium in a two-box model, and has biological processes with/without isotopic fractionation. We have applied this model to the Sea of Okhotsk and successfully reproduced the δ^{15}N of nitrate measured in seawater and the seasonal variations in δ^{15}N of sinking particles obtained from sediment trap experiments. Simulated δ^{15}N of phytoplankton are determined by δ^{15}N of nitrate and ammonium, and the nitrogen *f*-ratio, defined as the ratio of nitrate assimilation by phytoplankton to total nitrogenous nutrient assimilation. Detailed considerations of biological processes in the spring and autumn blooms have demonstrated that there is a significant difference between simulated δ^{15}N values of phytoplankton, which assimilates only nitrate, and only ammonium, respectively. We suggest that observations of δ^{15}N values of phytoplankton, nitrate and ammonium in the spring and autumn blooms may indicate the ratios of nutrient selectivity by phytoplankton. In winter, most of the simulated biogeochemical fluxes decrease rapidly, but nitrification flux decreases much more slowly than the other biogeochemical fluxes. Therefore, simulated δ^{15}N values and concentrations of ammonium reflect almost only nitrification. We suggest that the nitrification rate can be parameterized with observations of δ^{15}N of ammonium in winter and a sensitive study varying the parameter of nitrification rate.

Keywords:
· Nitrogen isotopes,
· ecosystem model,
· sediment traps,
· seasonal variation,
· Sea of Okhotsk.

1. Introduction

Incubation experiments with the artificial addition of ^{15}N tracers have been widely conducted to estimate the various marine biogeochemical fluxes and rates of nitrogenous nutrients. For example, uptake rates of nutrients and nitrogen *f*-ratios, defined as the ratio of nitrate assimilation by phytoplankton to total nitrogenous nutrient assimilation, have been estimated with on-deck and/or in-situ incubation experiments through assimilations of ^{15}N-nitrate, ^{15}N-ammonium or ^{15}N-urea by phytoplankton (e.g., Dugdale and Wilkerson, 1986; Sambrotto and Mace, 2000; Wilkerson *et al*., 2000; Sambrotto, 2001). Nitrification rates have been measured in in-situ incubation experiments through ^{15}N-ammonium oxidation (Sutka *et al*., 2004). These fluxes and rates are usually estimated with small bottles for a few hours, or up to two days at most. That is, the condition of the incubation experiment is restricted to a small space and a short time. Moreover, these experiments are difficult to conduct under the condition of the actual concentration of substrate, because artificial ^{15}N addition changes this concentration. In a strict sense, these are reasons why the

* Corresponding author. E-mail: c-yoshikawa@jamstec.go.jp
Present address: Frontier Research Center for Global Change, Japan Agency for Marine-Earth Science and Technology, Showamachi, Kanazawa-ku, Yokohama 236-0001, Japan.

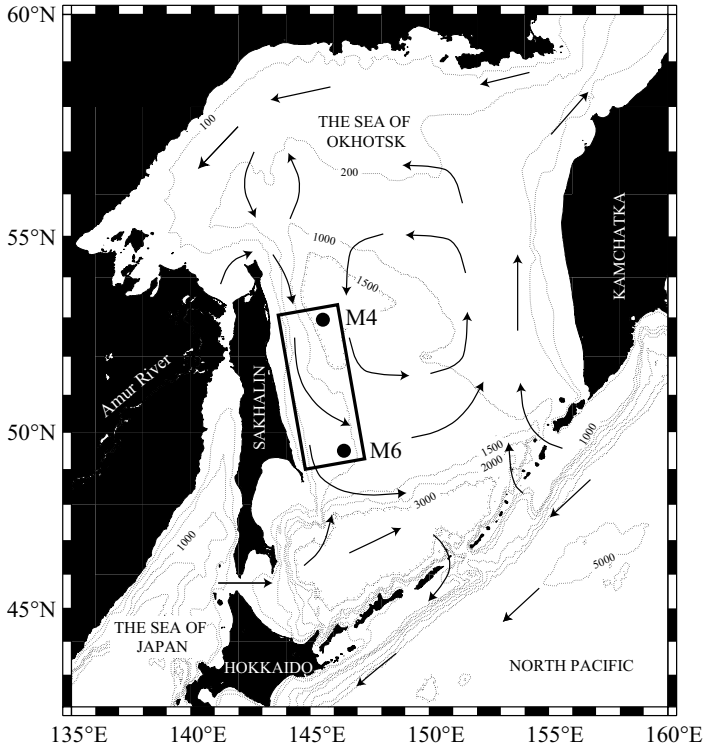

Fig. 1. Map of the Sea of Okhotsk and locations of the sediment trap mooring M4 and M6. Arrows show a pattern of the surface current. The square off the east coast of Sakhalin shows the region where our model is applied.

Table 1. Site information for sediment trap mooring.

Site	Lat.	Long.	Time period	Trap depth (m)	Depth of water (m)
M4	53°00′N	145°29′E	1998.8.7–1999.8.7	300	1754
	53°01′N	145°30′E	1999.9.8–2000.6.7	300	1756
M6	49°31′N	146°30′E	1998.8.7–1999.8.7	300	812
	49°31′N	146°29′E	1999.9.27–2000.6.7	300	804

incubation experiments cannot simulate a natural ecosystem. On the other hand, the natural abundance of nitrogen isotopes has also been observed to understand marine biogeochemical processes. For example, δ^{15}N values of nutrients in the surface water usually show the degree of nutrient utilization (e.g., Miyake and Wada, 1971; Altabet *et al.*, 1991; Waser *et al.*, 1998), and the relationship among δ^{15}N values of phytoplankton, zooplankton, fishes, marine mammals, etc., indicates the degree of trophic level (Minagawa and Wada, 1984; Wu *et al.*, 1997; Adams and Sterner, 2000). Moreover, δ^{15}N of nitrogenous components in a special region indicate the source of nutrients affected by denitrification or nitrogen fixation (Ostrom *et al.*, 1997; Altabet *et al.*, 1999), although these processes do not occur in the Sea of Okhotsk. These estimations are made under natural ecosystem conditions. However, little quantitative estimation has been done, since natural abundances of nitrogen isotopes are determined by complex biogeochemical processes. In this study, we not only use actual observed data of δ^{15}N, but also an ecosystem model including various biogeochemical processes and nitrogen isotopes to quantitatively understand nitrogen isotopic dynamics. Furthermore, we suggest a new potential of natural abundance of nitrogen isotopes as a tracer instead of the incubation experiment.

Observed δ^{15}N values of nitrogenous components record information concerning the marine biogeochemical cycle, as described above. However, δ^{15}N of nitrogenous components are hard to observe frequently throughout the

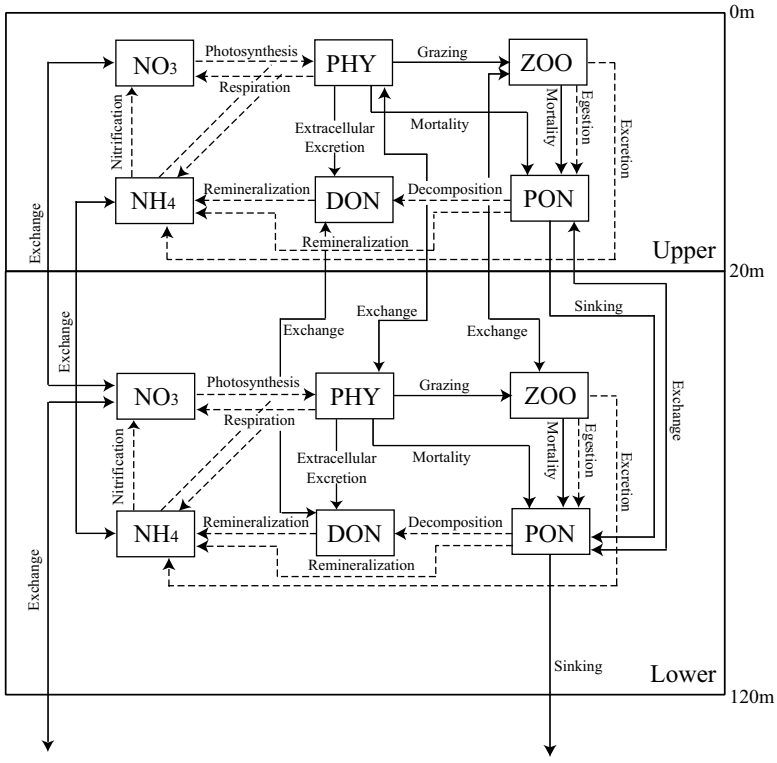

Fig. 2. Schematic view of interactions among the six model compartments in the upper (0–20 m deep) and lower (20–120 m deep) layers. The symbol NO_3 indicates nitrate concentration, NH_4 ammonium, PHY phytoplankton, ZOO zooplankton, PON particulate organic nitrogen, and DON dissolved organic nitrogen. Dashed and solid arrows indicate nitrogen flows with and without isotope fractionation, respectively.

year. To validate our model comparing the simulated $\delta^{15}N$ values and the observed data set, we are also in need of another recorder. Information of $\delta^{15}N$ in surface water is transmitted to $\delta^{15}N$ of sinking particles. Seasonal variations in $\delta^{15}N$ of the sinking particles obtained from sediment trap experiments can reproduce the seasonal variations in biogeochemical processes in surface water. $\delta^{15}N$ values of sinking particles reflect the proportion in the components of sinking particles, which consist of dead phytoplankton and zooplankton bodies, as well as fecal pellets (Voss *et al*., 1996; Wu *et al*., 1999; Peña *et al*., 1999), and the state of nutrients in the surface water, such as the degree of nutrient utilization (Altabet and Deuser, 1985; Altabet *et al*., 1991; Altabet and Francois, 1994, 2001; Voss *et al*., 1996; Nakatsuka and Handa, 1997; Peña *et al*., 1999). In this study we also compare the simulated $\delta^{15}N$ values of sinking particles with those observations in order to confirm our model's consistency with real seasonal variations in $\delta^{15}N$ of nitrogenous components.

We have developed an ecosystem model including nitrogen isotopes based on recent ecosystem models, which successfully simulated several time series observations in high latitudes (Kawamiya *et al*., 1997, hereafter KKYS; Fujii *et al*., 2002; Yamanaka *et al*., 2004, hereafter YYFANK). We apply this model to the region off the east coast of Sakhalin in the Sea of Okhotsk (Fig. 1; 49–53°N, 144–146°E). The Sea of Okhotsk is located at the northwestern rim of the North Pacific, where the maximum primary production reaches 5000 $mgC/m^2/day$, which is much higher than typical values of the northwestern Pacific (Sorokin and Sorokin, 1999). CTD observations and water sampling were taken in the Sea of Okhotsk during three research cruises by R/V Professor Khromov. Sediment trap experiments were also carried out at two mooring stations off the east coast of Sakhalin for two years (Table 1), where a seasonal variation in fluxes of sinking particles has been observed (Yoshikawa *et al*., 2001; Nakatsuka *et al*., 2004). These observations provide us with enough data (e.g., $\delta^{15}N$ of sinking particles and nitrate, fluxes of sinking particles, concentrations of nitrate, ammonium and chlorophyll-a) to construct and validate the ecosystem model (Yoshikawa *et al*., 2001, 2005; Nakatsuka *et al*., 2004).

2. Model Description

The ecosystem model in this study has six compart-

Table 2. Biological parameters.

V_{max}	Phytoplankton Maximum Photosynthetic Rate at 0℃	0.5	/day
K_{NO_3}	Phytoplankton Half Saturation Constant for Nitrate	2	μmolN/l
K_{NH_4}	Phytoplankton Half Saturation Constant for Nitrate	0.2	μmolN/l
Ψ	Phytoplankton Ammonium Inhibition Coefficient	1.5	l/μmolN
k	Phytoplankton Temperature Coefficient for Photosynthetic	0.0693	/℃
I_{opt}	Phytoplankton Optimum Light Intensity	104.7	W/m^2
M_{p0}	Phytoplankton Mortality Rate at 0℃	0.04375	l/μmolN/day
k_{Mp}	Phytoplankton Temperature Coefficient for Mortality	0.0693	/℃
R_{p0}	Phytoplankton Respiration Rate at 0℃	0.03	/day
k_R	Phytoplankton Temperature Coefficient for Respiration	0.0519	/℃
γ	Phytoplankton Ratio of Extracellular Excretion to Photosynthesis	0.135	(nodim.)
G_{Rmax}	Zooplankton Maximum Grazing Rate at 0℃	0.3	/day
k_G	Zooplankton Temperature Coefficient for Grazing	0.0693	/℃
l	Zooplankton Ivlev Constant	1.4	l/μmolN
P^*_Z	Zooplankton Threshold Value for Grazing	0.04	μmolN/l
α	Zooplankton Assimilation Efficiency	0.7	(nodim.)
β	Zooplankton Growth Efficiency	0.3	(nodim.)
M_{z0}	Zooplankton Mortality Rate at 0℃	0.0585	l/μmolN/day
k_{Mz}	Zooplankton Temperature Coefficient for Mortality	0.0693	/℃
α_1	Light Dissipation Coefficient of Sea Water	0.04	/m
α_2	Self Shading Coefficient	0.04	l/μmolN/m
S_{PON}	PON sinking Velocity	20	m/day
k_{Nit}	Nitrification Rate at 0℃	0.03	/day
N_{Nit0}	Temperature Coefficient for Nitrification	0.0693	/℃
V_{PA0}	Remineralization Rate of PON to Ammonium at 0℃	0.1	/day
k_{PA0}	Temperature Coefficient for PON Remineralization to Ammonium	0.0693	/℃
V_{PD0}	Decomposition Rate of PON to DON at 0℃	0.1	/day
k_{PD}	Temperature Coefficient for POM Decomposition to DON	0.0693	/℃
V_{DA0}	Remineralization Rate of DON to Ammonium at 0℃	0.2	/day
k_{DA}	Temperature Coefficient for DON Remineralization to Ammonium	0.0693	/℃

The equations of each processes with these parameters are reported in Yamanaka *et al.* (2004).

ments, the prognostic variables being concentrations of nitrogen (N). Figure 2 illustrates the six compartments, phytoplankton (PHY), zooplankton (ZOO), particulate organic nitrogen (PON), dissolved organic nitrogen (DON), nitrate (NO_3) and ammonium (NH_4). The equations for the nitrogen cycle are the same as those in KKYS and are presented in detail in Appendix A.1. Photosynthesis is formulated as a function of light intensity, temperature and concentrations of nitrate and ammonium. The other biological processes are formulated as functions of temperature and nitrogen concentrations. The PON in this model consists of dead phytoplankton and zooplankton bodies and fecal pellets of zooplankton. The parameters are based on those in YYFANK applied to the northwestern Pacific, since the ecosystem there is similar to that in the Sea of Okhotsk (Table 2). As YYFANK has two classes of phytoplankton and two species of zooplankton, parameters for planktons in our model are set to the mean values of those of the small and large classes.

We added the ^{15}N (nitrogen isotope) cycle to the nitrogen cycle in KKYS. The ^{15}N concentrations of the six compartments are also prognostic variables, and their equations are presented in detail in Appendix A.2. Isotopic fractionation of each process has been studied as follows. Phytoplankton assimilates mainly nitrate and ammonium as its nitrogen source. Since $^{14}NO_3^-$ and $^{14}NH_4^-$ are more readily assimilated than $^{15}NO_3^-$ and $^{15}NH_4^-$, the $\delta^{15}N$ of nitrate and ammonium in the surface water increase as phytoplankton takes up these nutrients (e.g., Miyake and Wada, 1971; Altabet *et al.*, 1991; Waser *et al.*, 1998). The isotopic fractionation during uptake of nitrate by phytoplankton is estimated to be from –4 to

Table 3. Nitrogen isotope effects (ε) in biogeochemical processes.

Process	ε (‰)	Remarks
NO_3^- assimilation by phytoplankton	$\varepsilon_1 = -5$	in field –5 (Wada, 1980) –7 (Horrigan *et al.*, 1990) –5~–6 (Wu *et al.*, 1997) –4~–6 (Sigman *et al.*, 1999) –5 (Altabet *et al.*, 1999) –6~–8 (Altabet *et al.*, 2001) in culture 0~–15 (Montoya and McCarthy, 1995) –2~–6 (Waser *et al.*, 1998)
NH_4^+ assimilation by phytoplankton	$\varepsilon_2 = -10$	in field –9 (Cifuentes *et al.*, 1989) –7~–8 (Montoya *et al.*, 1991) in culture –5~–29 (Pennock *et al.*, 1996) –16~–26 (Waser *et al.*, 1998)
Excretion by zooplankton	$\varepsilon_3 = -5$	–2~–8 (Checkley and Miller, 1989)
Egestion by zooplankton	$\varepsilon_4 = -2$	no data
Nitrification	$\varepsilon_5 = -14$	–5~–21 (Miyake and Wada, 1971) –12~–17 (Horrigan *et al.*, 1990) –14~–38 (Casciotti *et al.*, 2003)
Remineralization (PON to NH_4^+)	$\varepsilon_6 = -1$	no data
Remineralization (DON to NH_4^+)	$\varepsilon_7 = -1$	no data
Decomposition (PON to DON)	$\varepsilon_8 = -1$	0~–2 (Miyake and Wada, 1971)

–8‰ in the field (Wada, 1980; Horrigan *et al.*, 1990; Wu *et al.*, 1997; Sigman *et al.*, 1999; Altabet *et al.*, 1999) and from –2 to –15‰ in culture (Montoya and McCarthy, 1995; Waser *et al.*, 1998). As for ammonium, the isotope fractionation is estimated to be from –6.5 to –9.1‰ in the field (Cifuentes *et al.*, 1989; Montoya *et al.*, 1991) and from –5 to –29‰ in culture (Pennock *et al.*, 1996; Waser *et al.*, 1998). The ammonium excreted by zooplankton is lighter, by 2 to 8‰, than the concentration of their bodies (Checkley and Miller, 1989), but their fecal pellets are roughly 1‰ heavier than the diet (Altabet and Small, 1990; Montoya *et al.*, 1990). The net result of these two processes is an increase in δ^{15}N of animal tissue relative to the animal's diet. An average increase of 3.4‰ (ranging from 0 to 6‰) per trophic level was estimated in previous studies (Minagawa and Wada, 1984; Wu *et al.*, 1997; Adams and Sterner, 2000). The enrichment in δ^{15}N of PON associated with microbial degradation has been inferred in many studies (Saino and Hattori, 1980, 1987; Altabet and McCarthy, 1985; Ostrom *et al.*, 1997). PON is known to be decomposed to ammonium by microbial processes. The fractionation of ammonification is estimated to be from 0 to –5‰ (Miyake and Wada, 1971; Hoch *et al.*, 1996; Ostrom *et al.*, 1997; David, 2001). Ammonium is oxidized to nitrate by nitrifying bacteria. The fractionation for nitrification is estimated to be from –5 to –38‰ (Miyake and Wada, 1971; Horrigan *et al.*, 1990; Casciotti *et al.*, 2003), which is larger than the other indicated values. The isotopic fractionation effect (ε (‰)) for each process is set to a mean value within the range of the following effects, as in previous studies (Table 3). For the representation and discussion in this paper, we use the traditional notation, δ^{15}N, converted from ^{15}N concentrations, although these values are calculated in the model. The δ^{15}N value is defined as $\delta^{15}\mathrm{N}\ (‰) = ((^{15}\mathrm{N}/^{14}\mathrm{N})_{\mathrm{sample}}/(^{15}\mathrm{N}/^{14}\mathrm{N})_{\mathrm{atmospheric\ N2}} - 1) \times 1000$ using ^{15}N and ^{14}N of each compartment.

We applied the box model including the biological processes described above to regions off the east coast of Sakhalin in the Sea of Okhotsk (Fig. 1). This model has two vertical layers (Fig. 2). In this region, mixed layer depths, which are given in reference to the observed ver-

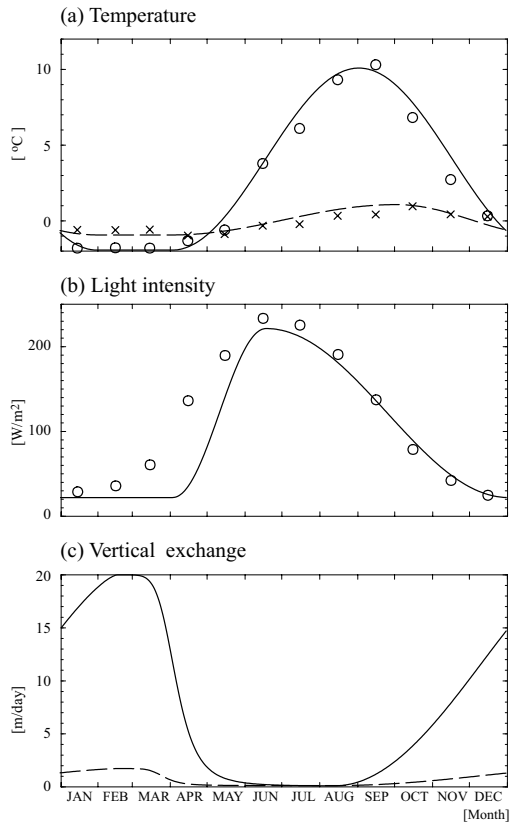

Fig. 3. Seasonal variations: (a) water temperature simulated in the upper layer (solid line) and the lower layer (dashed line) and obtained from WOA94 in the upper (○) and lower layers (×), (b) solar radiation simulated (solid line) and obtained from NCEP (open circle), and (c) the coefficient of water exchange between the upper and lower layers (g_1: solid line) and between the lower layer and layer deeper than 120 m (g_2: dashed line).

tical distribution of monthly temperature, show a minimum value of 20 m in summer and a maximum value of 120 m in winter. The boundary depth between the upper and lower boxes and the bottom boundary depth are set to the minimum and maximum mixed layer depths, respectively. To represent seasonal variations of the mixed layer, the values of water exchanges between the upper and lower layers (g_1) and between the lower layer and that deeper than 120 m (g_2) are changed seasonally (Fig. 3). The sensitivities of g_1 and g_2 are discussed in Appendix A.1. Boundary conditions for the nitrate concentration and its $\delta^{15}N$ value at 120 m depth are fixed to 23 μmol/l and 6‰, respectively, which are the means of the observations from 1998 to 2000. The East Sakhalin Current flows southward along the east coast of Sakhalin (Ohshima *et al.*, 2002). The data also reveal a flow to the south of approximately 0.3 m/s in winter and 0.05 m/s in summer at the mooring stations (Mizuta *et al.*, 2003). However, horizontal advection is ignored, since the contribution of horizontal advection, which is estimated from the horizontal gradients of observed nitrate concentrations at the north and south sides of the domain applied our model, is much smaller than seasonal changes in the surface nitrate concentration. The water temperature used in the equations for biological processes is interpolated from the monthly values in the World Ocean Atlas 94 (WOA94) climatology data (Fig. 3). The solar radiation is obtained from the monthly mean from 1998 to 1999 in the National Center for Environmental Prediction (NCEP) data set by interpolation, except for the period when the region is covered with seasonal sea ice. Only in the period when the region is covered with seasonal sea ice, is the radiation fixed to the winter minimum NCEP data of 20 Wm^{-2}. Under climatological forcings, we repeat the annual cycle four times to obtain a quasi-steady state. We compare the last two years with the observations from August 1998 through to July 2000.

3. Calculated Results in the Control Case

Figure 4 shows seasonal variations in primary production, the flux of sinking particulate organic nitrogen and concentrations of chlorophyll-a, zooplankton, nitrate, ammonium and dissolved organic nitrogen. Simulated primary production and chlorophyll-a concentration calculated with the phytoplankton concentration have two peaks. These peaks are typical of the Sea of Okhotsk (Honda *et al.*, 1997; Yoshikawa *et al.*, 2001; Nakatsuka *et al.*, 2004) and correspond to phytoplankton blooms, which occurs in spring and autumn. The simulated peak of primary production in the autumn bloom is higher than in the spring bloom, although the simulated peak of chlorophyll-a concentration in the autumn bloom is smaller than in the spring bloom. The reason for this difference is that temperature in the autumn bloom is higher by about 8°C than that in the spring, and therefore the ratio of photosynthesis flux to PHY concentration in the autumn bloom is about 1.7 times as high as that in the spring bloom. The rates of primary production are about 2200 $mgC/m^2/day$ in spring and 2400 $mgC/m^2/day$ in autumn, and about 700 $mgC/m^2/day$ from July to August. During the cruises in July to August 1992 (Sorokin and Sorokin, 1999), the maximum primary production in the Sea of Okhotsk in patches of bloom reached 5000 $mgC/m^2/day$, and primary productions after the spring bloom in the region off Sakhalin were 570 to 1330 $mgC/m^2/day$. The simulated primary productions are within the observed range reported in a previous study. The simulated chlorophyll-a concentration is about 5 μgChl-a/l in spring and 3 μgChl-a/l in autumn at the upper layer (Fig. 4(b)). The simulated chlorophyll-a in the spring bloom is within the observed range. Observed chlorophyll-a concentration in

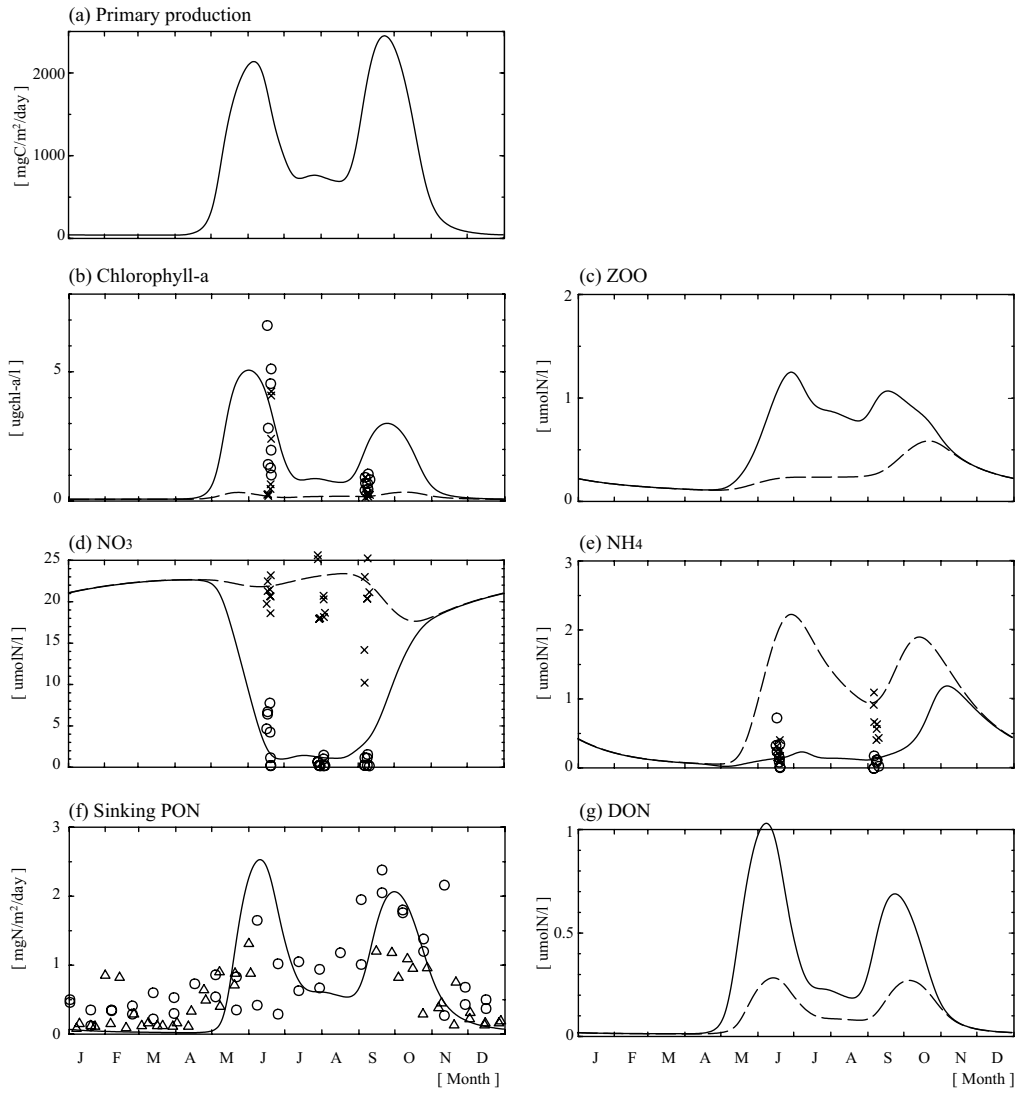

Fig. 4. Seasonal variations: (a) simulated primary production, (b) chlorophyll-a concentrations simulated in the upper and lower layers and observed in the upper and lower layers, (c) ZOO concentrations simulated in the upper and lower layers, (d) NO_3 concentrations simulated and observed in the upper and lower layers, (e) NH_4 concentrations simulated and observed in the upper and lower layers, (f) sinking PON fluxes simulated at 300 m deep and observed from August 1998 to August 1999 (open circle) and from September 1999 to June 2000 (open triangle) at both M4 and M6 sites (Yoshikawa *et al*., 2001; Nakatsuka *et al*., 2004) and (g) DON concentrations simulated in the upper and lower layers. Solid and dashed lines and symbols ○ and × are the simulated and observed values, respectively, in the upper and lower layers. The observed data are collected by three cruises, conducted in June 2000, from July to August 1998 and in September 1999, in the region where our model is applied. Simulated chlorophyll-a concentrations are calculated using the nitrogen-chlorophyll ratio of 1:1.325. To compare simulated fluxes of sinking particles with the observation by sediment traps at 300 m deep, the simulated fluxes of sinking particles in (f) are estimated by the effect of decomposition with sinking from 120 m to 300 m depth, multiplied by 1/3, and by the trapping efficiencies of sediment traps, multiplied by 15%, due to strong currents. These traps collect sinking particles at about two week intervals.

June 2000 is widely scattered, because some observation points fall during the spring bloom stage and have high chlorophyll-a and nitrate concentrations, whereas others occur after the spring bloom, and therefore have low concentrations. Observed chlorophyll-a in early September 1999 is lower than that of simulation. This is because the observation in 1999 was conducted before the beginning of the bloom (Yoshikawa *et al*., 2001; Nakatsuka *et al*., 2004). The autumn bloom in 1999 is also much weaker than that in 1998, estimated from sediment trap and the

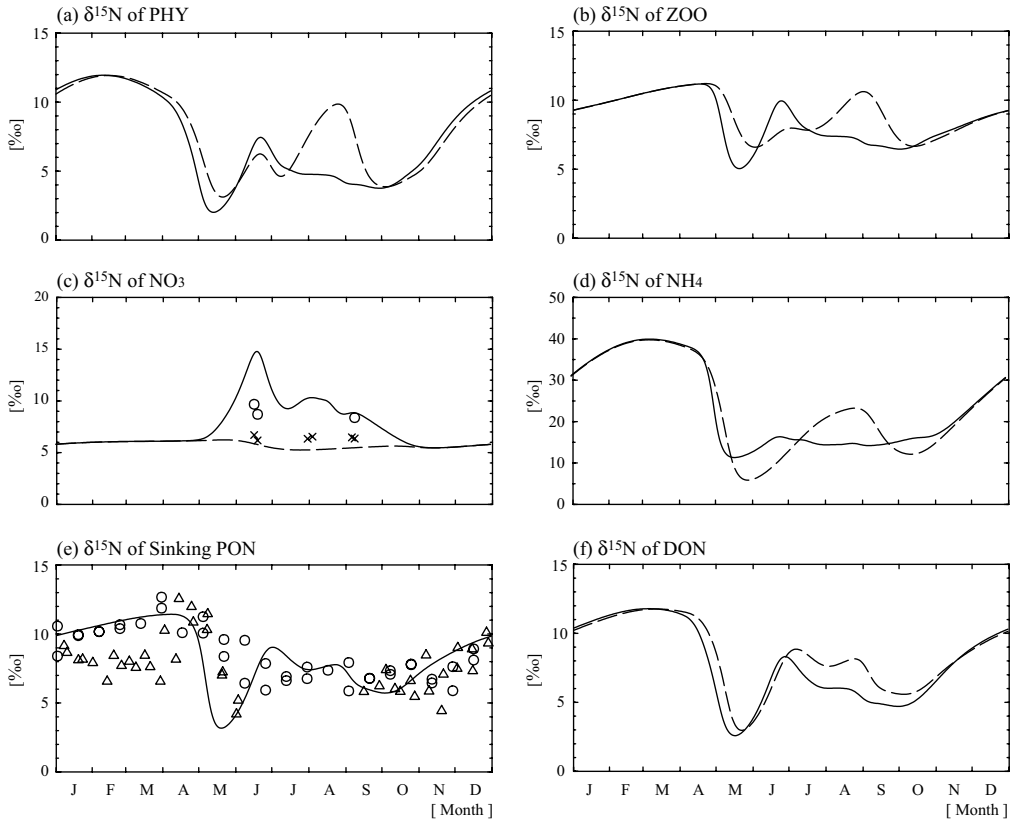

Fig. 5. Seasonal variations: (a) δ^{15}N values of PHY simulated in the upper and lower layers, (b) δ^{15}N values of ZOO simulated in the upper and lower layers, (c) δ^{15}N values of NO_3 simulated and observed in the upper and lower layers by Yoshikawa *et al.* (2004), (d) δ^{15}N values of NH_4 simulated in the upper (solid line) and lower layers, (e) δ^{15}N values of simulated sinking PON and observed from August 1998 to August 1999 (open circle) and from September 1999 to June 2000 (open triangle) by Yoshikawa *et al.* (2001) and (f) δ^{15}N values of DON simulated in the upper and lower layers. Solid and dashed lines and symbols ○ and × are the simulated and observed values, respectively, in the upper and lower layers. The observed data are collected by three cruises, which were conducted in June 2000, from July to August 1998 and in September 1999, in the region where our model is applied.

SeaWiFS data (Fukuda, personal communication), although the chlorophyll-a during the bloom in 1998 was not measured, unfortunately. The simulated chlorophyll-a in the autumn bloom roughly reproduces the observed level before the beginning of the bloom.

Figures 4(d) and (e) show the seasonal variations in nutrient concentrations of nitrate and ammonium. The simulated nitrate concentration in the upper layer decreases during the spring bloom, and in summer it is depleted to about 1 μmol/l. The simulated nitrate increases in autumn, because of the presence of a supply of water with large amounts of nitrate below. Strong convective mixing during winter keeps the simulated nitrate concentrations in the upper and lower layers very close to the values in the layer below 120 m (23 μmol/l). The ammonium concentration in the lower layer peaks one month after the spring and autumn blooms, when PON produced during the blooms is remineralized and zooplankton excrete ammonium. On the other hand, the peak in the upper layer is very small, because ammonium is rapidly consumed by photosynthesis. In winter, the ammonium accumulated from summer to autumn is consumed by nitrification, as discussed in Section 5. The concentrations of nutrients in our model successfully reproduce the observed nutrient concentrations. Figure 4(f) shows the seasonal variations in the flux of sinking PON in comparison with data from the sediment trap experiments at 300 m depth. The flux of sinking PON has two peaks corresponding to spring and autumn blooms, as well as the primary production and chlorophyll-a concentration. The collected sinking particles in sediment trap experiments show maxima occurring in September 1998, June 1999, September 1999 and May 2000. As mentioned before, the observed autumn bloom in 1998 is strong, but that in 1999 is weak. From January to March in 2000, some of the observed fluxes are slightly high, due to contamination

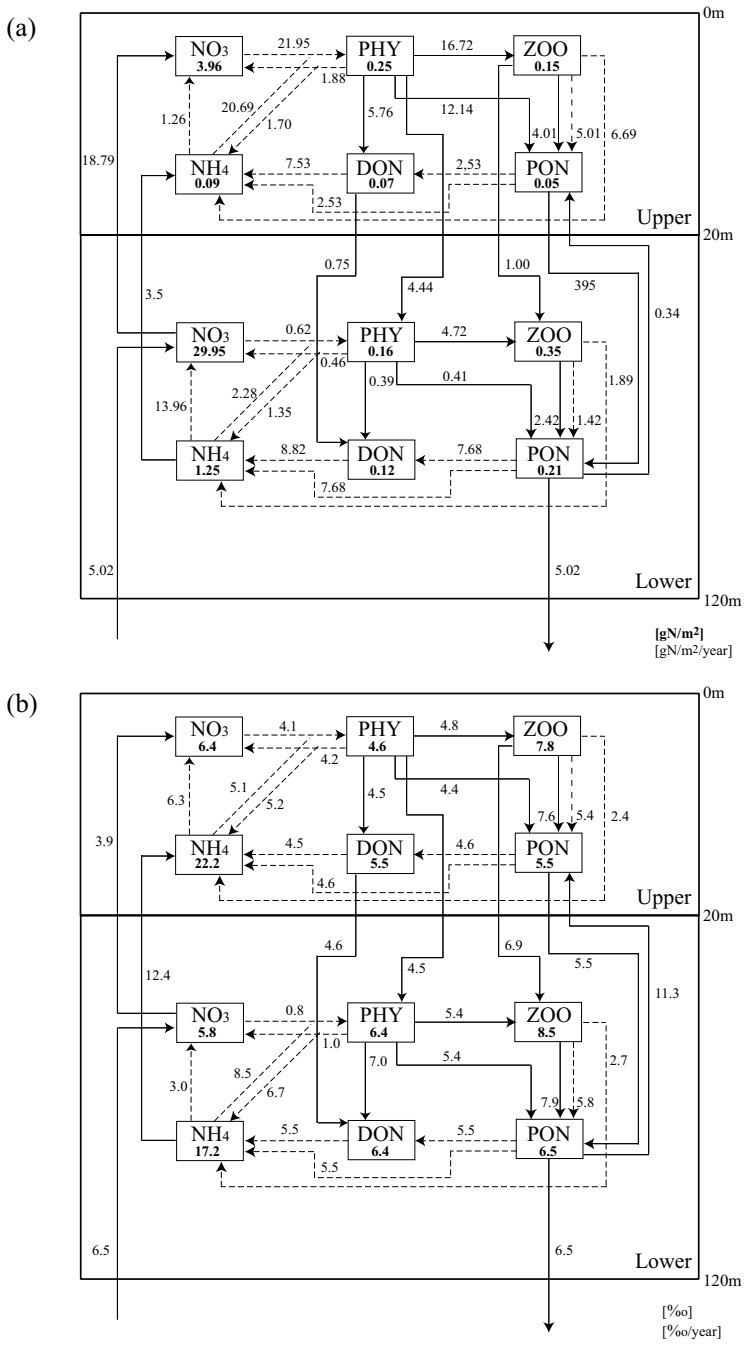

Fig. 6. Budgets for one year: (a) nitrogen cycling and (b) ^{15}N cycling. Bold fonts indicate the average column-integrated nitrogen masses per 1 m^2 (gN/m^2) (a) and the average $\delta^{15}N$ values (‰) (b) for one year of each compartment. Regular fonts indicate nitrogen budgets (gN/m^2/year) in (a) and their $\delta^{15}N$ values (‰) in (b) for one year.

by resuspended matter from the ocean floor (Nakatsuka *et al.*, 2004). Simulated seasonal variations in fluxes of sinking particles almost reproduce the observed seasonal variations.

Next, in Fig. 5, we see the seasonal variations in the $\delta^{15}N$ values of phytoplankton, zooplankton, nitrate, ammonium, particulate organic nitrogen and dissolved organic nitrogen. All compartments, except nitrate, show low $\delta^{15}N$ values from spring to autumn, and high $\delta^{15}N$ values in winter. The seasonal variations of nitrate in our model successfully reproduce the observations from spring to autumn (Fig. 5(c)). During the spring bloom,

the simulated $\delta^{15}N$ of nitrate in the upper layer increases as its concentration decreases, because phytoplankton assimilates $^{14}NO_3^-$ more readily than $^{15}NO_3^-$. In summer, the simulated $\delta^{15}N$ of nitrate in the upper layer shows a high value of about 10‰, and its concentration is near zero. The simulated $\delta^{15}N$ values of nitrate in autumn decreases, because water with large amounts of low-$\delta^{15}N$ nitrate is supplied from below. We predict from the simulation that strong convective mixing during winter keeps the $\delta^{15}N$ of nitrate in the upper and lower layers very close to 6‰ in the layer below 120 m, although we could not observe $\delta^{15}N$ of nitrate in winter. The seasonal variations in the $\delta^{15}N$ values of sinking particles in our model almost reproduce the observed variations (Fig. 5(e)). At the start of the spring bloom, the simulated $\delta^{15}N$ values of sinking particles decrease rapidly from 11 to 3‰. This is because PON becomes rich in phytoplankton with lower $\delta^{15}N$ than zooplankton, and because this phytoplankton assimilates mainly nitrate with lowest $\delta^{15}N$ in a year. At the latter half of the spring bloom, $\delta^{15}N$ values of sinking particles increase, because $\delta^{15}N$ of nitrate and phytoplankton become high due to preferential uptake of $^{14}NO_3$ by phytoplankton. The $\delta^{15}N$ values of sinking particles maintains low values of about 7‰ during summer and gradually increases to about 12‰ from autumn to winter. The observed sinking particles from January to March in 2000 are not consistent with the simulated values of 10‰, because these values are contaminated by resuspended matter from the ocean floor, and the $\delta^{15}N$ shifts to about 7‰, which is the value for surface sediments in this region (Ohnishi, personal communication).

Figure 6(a) represents a nitrogen budget in our model for one year. The sum of simulated primary production in the upper and lower layers is 45.54 gN/m^2/year (301 gC/m^2/year), which is much higher than the observed average of the northwestern Pacific (Imai *et al.*, 2002 (KNOT: 89 gC/m^2/year)). This result is consistent with the previous observed primary production in the Sea of Okhotsk, which is much higher than that in the northwestern Pacific (Sorokin and Sorokin, 1999). The simulated production of PON is 25.41 gN/m^2/year, which is about 56% of simulated primary production. As nearly 80% of the PON is degraded above the 120 m depth in our model, simulated export production is only 5.02 gN/m^2/year. Thus, the e-ratio calculated from the ratio of simulated export production to simulated primary production is about 0.11. Of the total primary production, the simulated nitrate uptake is 22.57 gN/m^2/year, and the simulated ammonium uptake is 22.97 gN/m^2/year. Hence, the *f*-ratio calculated from the ratio of simulated nitrate uptake to simulated total nitrogen uptake (nitrate + ammonium), is about 0.50, and this value is similar to previous model studies in the northwestern Pacific (Fujii *et al.*, 2002 (KNOT: 0.58); YYFANK (A7: 0.60)). The simulated uptakes of nitrate supplied from the layer deeper than 120 m and nitrified from ammonium are 5.02 gN/m^2/year and 15.22 gN/m^2/year, respectively, which are 11% and 33% of the total nitrogen uptake. Therefore, regeneration including nitrification above 120 m depth is 89% of the simulated total nitrogen uptake. It is important to consider, not only regeneration in the upper layer, but also the following cycle: PON in the upper layer sinks to the lower layer, and is remineralized and nitrified to nitrate, which is then transported to the upper layer.

Figure 6(b) shows a ^{15}N budget in our model for one year. The annual average of simulated $\delta^{15}N$ of phytoplankton above the depth of 120 m, weighted by the column-integrated nitrogen masses of PHY in the upper and lower boxes (see Fig. 6(a)), is 5.3‰, the minimum among the six compartments. This is due to the large isotopic fractionations at the inflows to PHY, which are –5‰ and –10‰ during nitrate and ammonium uptakes, respectively (Table 3), and also the absence of isotopic fractionations at the outflows from PHY. The annual average of simulated $\delta^{15}N$ of zooplankton above the 120 m depth is 8.3‰, which is 3.0‰ higher than that of phytoplankton, because of there are no isotopic fractionations at the inflows to ZOO, and large isotopic fractionations at the outflows from ZOO, which are –5‰ and –2‰ during excretion and egestion by zooplankton, respectively (Table 3). The annual average of simulated $\delta^{15}N$ of ammonium above the depth of 120 m is 17.5‰, the maximum among the six compartments, since the isotopic fractionations at the outflows from NH_4, which are –14‰ and –10‰ during nitrification and ammonium uptake by phytoplankton, respectively, are much larger than the those at the inflows to NH_4, which are –1‰ at both decomposition and remineralization (Table 3). The weighted average of simulated $\delta^{15}N$ values and the sum of the inflows to each compartment are equal to those of the outflows from each compartment. The simulated $\delta^{15}N$ and flux of sinking PON are equal to the values of water exchange between the lower layer and the layer below 120 m, those being 6.5‰ and 5.02 gN/m^2/year, respectively. This model is therefore in a quasi-steady state.

4. Case Studies

Our model successfully reproduced observed seasonal variations in $\delta^{15}N$ and concentrations of biological components, as discussed in the previous section. However, some defects and restrictions may be hidden in our model, which were not found by the comparison between the simulation and observation. To confirm that our model is suitable for the simulation of the seasonal $\delta^{15}N$ variations in surface water, we conducted two case studies on comparison with the generalized model and the sensitivity of isotopic fractionation effects.

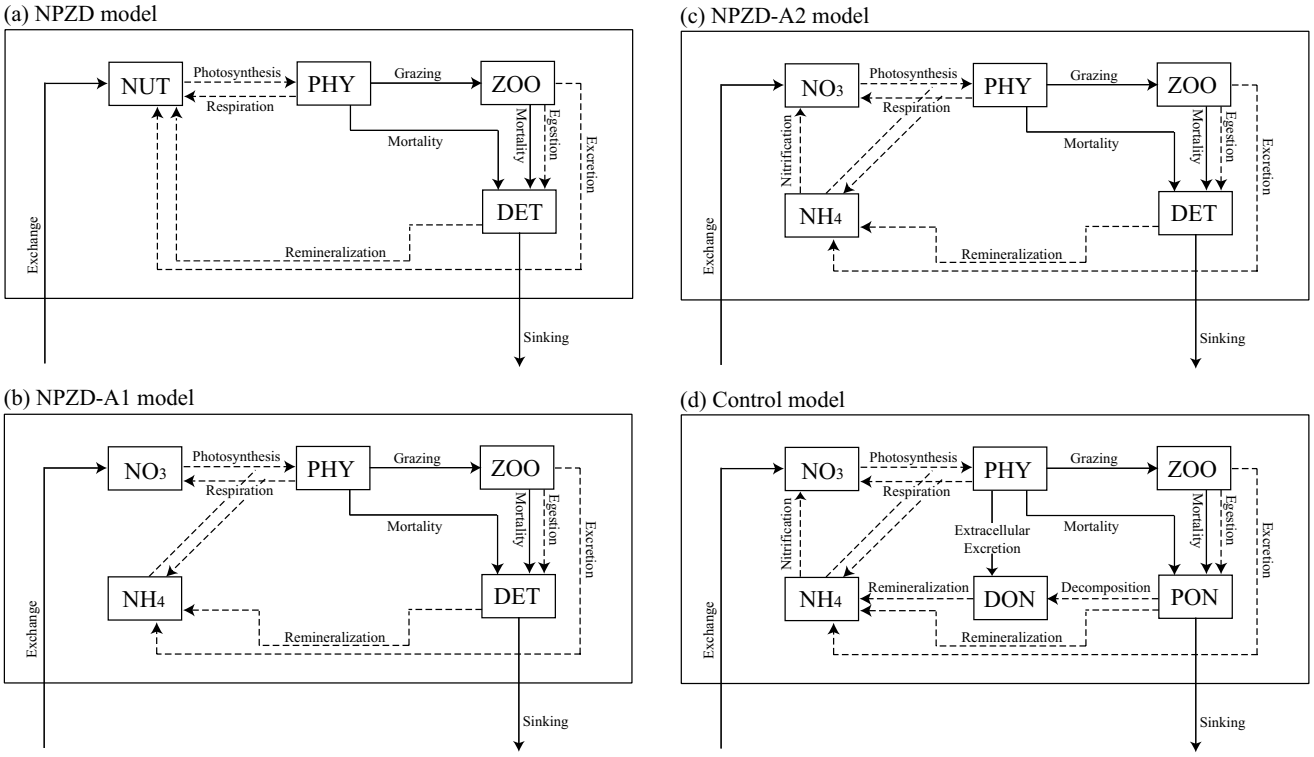

Fig. 7. Schematic view of interactions among the compartments of four model stages: (a) NPZD model, (b) NPZD-A1 model, (c) NPZD-A2 model and (d) control model (explanations of these stages are presented in the text). The symbols NUT indicate nutrients concentration, NO_3 nitrate, NH_4 ammonium, PHY phytoplankton, ZOO zooplankton, DET detritus, PON particulate organic nitrogen, and DON dissolved organic nitrogen. Dashed and solid arrows indicate nitrogen flows with and without isotope fractionation, respectively.

4.1 Comparison of our model with a generalized model

Giraud *et al.* (2000) developed a simple ecosystem model for a simulation of $\delta^{15}N$ of sediments. Their model, which consists of four compartments (PHY, ZOO, detritus and nutrients), is a typical generalized ecosystem model (e.g., Oschlies and Garçon, 1999; Giraud *et al.*, 2000, 2003; Waniek, 2003). It does not distinguish ammonium from nutrients. Assimilation and nitrification of ammonium with its large isotopic fractionation is not included in their model, although it should contribute to $\delta^{15}N$ of marine biological components in surface water. Therefore, we developed a six-compartment model, which consists of PHY, ZOO, PON, DON, NO_3 and NH_4, and thoroughly examined seasonal variations in $\delta^{15}N$ of sinking particles. To understand the difference between the generalized four-compartment model and ours of six, and to investigate the sensitivity of the biogeochemical processes involving ammonium, we conduct case studies using the following models: the generalized model (NPZD model in Fig. 7(a)), a model with ammonium and ammonium assimilation by phytoplankton added to the NPZD model (NPZD-A1 model in Fig. 7(b)), a model with nitrification added to the NPZD-A1 model (NPZD-A2 model in Fig. 7(c)), and a model with DON and associated processes added to the NPZD-A2, which is the same as our original model (control model in Fig. 7(d)).

Figures 8(a) and (b) show comparisons of seasonal variations in the fluxes and $\delta^{15}N$ values of sinking particles at 120 m depth as simulated by each of the four models. In all cases, the fluxes of sinking particles represent the observed two peaks in spring and autumn, except the maximum in July of the NPZD-A1 (Fig. 8(a)). The $\delta^{15}N$ of sinking particles also reproduce the observed variations from spring to summer (Fig. 8(b)). However, in the cases of NPZD and NPZD-A1 models, the $\delta^{15}N$ of sinking particles does not show the observed increase from autumn to winter (Fig. 8(b)). Previous studies explained the high $\delta^{15}N$ of sinking particles in winter as a result of particulate matter production by zooplankton, which have a $\delta^{15}N$ about 3‰ higher than that of phytoplankton (Altabet *et al.*, 1991; Voss *et al.*, 1996; Peña *et al.*, 1999; Altabet and Francois, 2001). Although these two models include the effects of zooplankton, the $\delta^{15}N$ of sinking particles of these cases in winter show the minimum in a

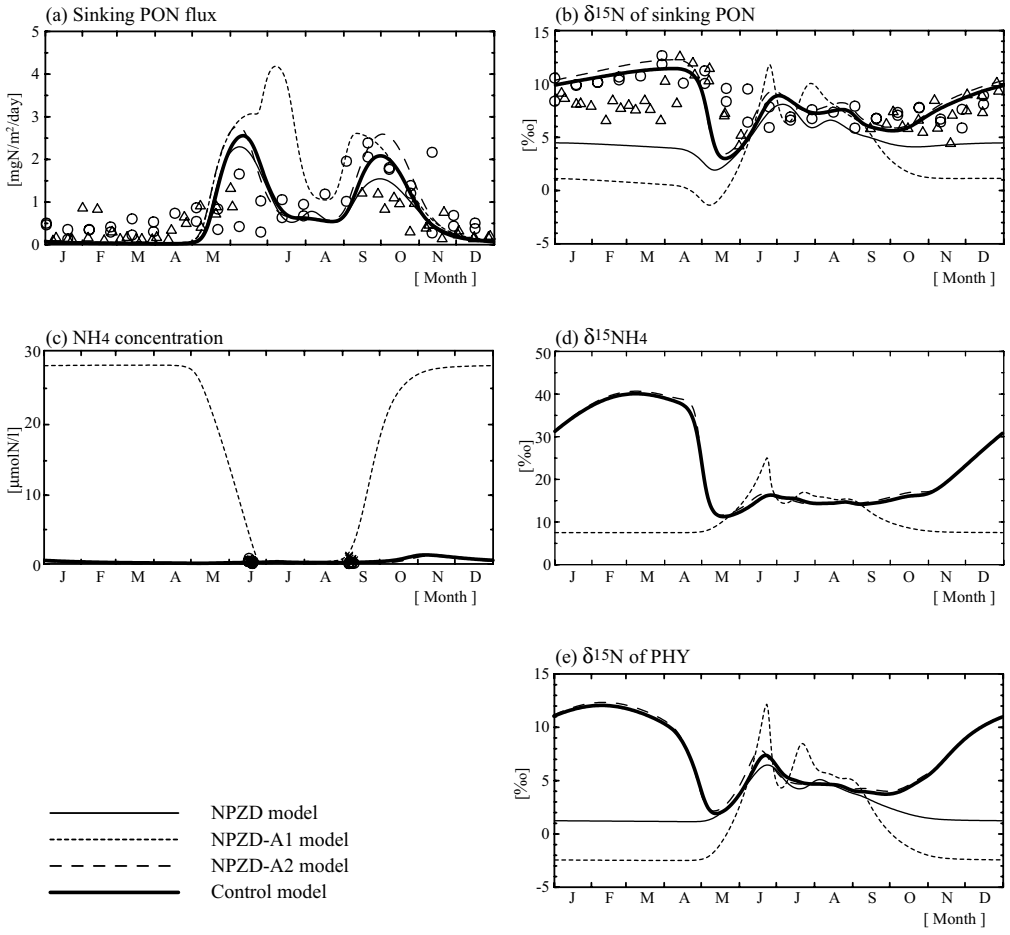

Fig. 8. Comparisons of the seasonal variations in: (a) fluxes of sinking PON, (b) δ^{15}N of sinking PON, (c) concentrations of ammonium, (d) δ^{15}N of ammonium and (e) δ^{15}N of phytoplankton as simulated by each of the four models. Thin, dotted, dashed and bold lines are the values in the model cases of NPZD (Fig. 7(a)), NPZD-A1 (Fig. 7(b)), NPZD-A2 (Fig. 7(c)) and control (Fig. 7(d)), respectively. Open circles and triangles indicate observed vales of sinking particles from August 1998 to August 1999 and from September 1999 to June 2000, respectively.

year. There seem to be other factors that maintain the high δ^{15}N of sinking particles in winter.

Figures 8(c), (d) and (e) show comparisons of seasonal variations in the concentrations and δ^{15}N values of ammonium from the three models, except the NPZD model and δ^{15}N values of phytoplankton from the four models, respectively. In the case of the NPZD-A1 model, which added ammonium to the NPZD model, the δ^{15}N of ammonium has its annual minimum in winter, which does not agree with the results from the NPZD-A2 and control models and observations (Fig. 8(d)). This is because only the nitrification with its large isotopic fractionation (included in the NPZD-A2 and control models) affects the winter δ^{15}N of ammonium, and the other processes affecting the δ^{15}N values of ammonium show extremely low fluxes, as discussed in detail in the next section. On the other hand, the NPZD-A1 model does not include nitrification and, therefore, δ^{15}N and concentrations of ammonium in winter from the NPZD-A1 model are low and unrealistically high, respectively. In the first half of the spring bloom in May, phytoplankton in the NPZD-A1 model mainly assimilates not nitrate but ammonium, due to the inhibition of nitrate assimilation by the high concentration of ammonium. In the last half of the bloom, nitrate remains in the surface water, although ammonium is exhausted by phytoplankton. Thus, the fluxes of sinking particles show a maximum in July, which is not consistent with the observation (Figs. 8(a) and (c)). In the autumn bloom, phytoplankton mainly assimilates not nitrate supplied by the winter convective mixing, but ammonium accumulated by the spring bloom. Therefore, the fluxes of sinking particles in the autumn bloom show an earlier maximum than that in the other cases. Moreover, δ^{15}N of phytoplankton in the NPZD and NPZD-A1 mod-

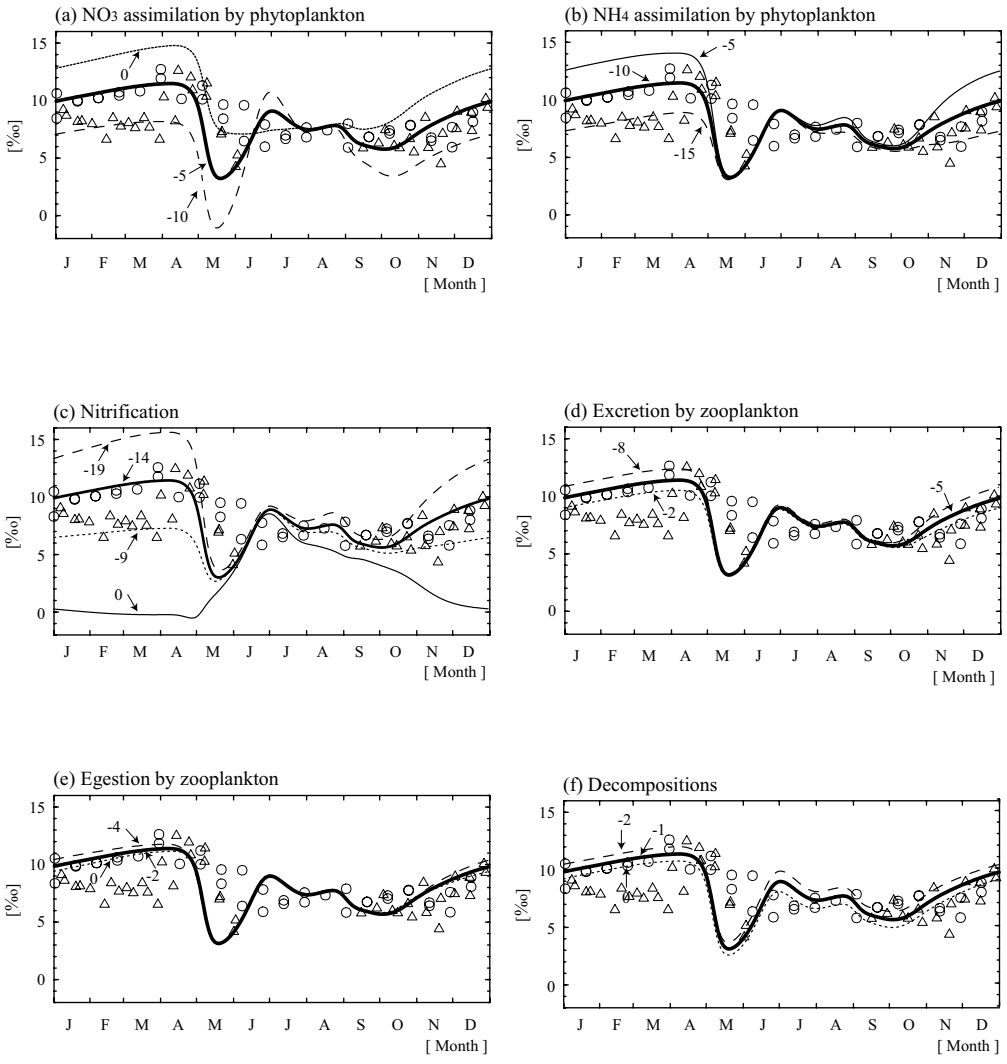

Fig. 9. Comparison of δ^{15}N of sinking particles among experiments changing the isotopic fractionation effects within the range measured in previous studies: (a) nitrate assimilation by phytoplankton of the small case of 0‰, the control case of –5‰ and the large case of –10‰, (b) ammonium assimilation by phytoplankton of the small case of –5‰, the control case of –10‰ and the large case of –15‰, (c) nitrification of the small case of –9‰, the control case of –14‰, the large case of –19‰ and the non-fractionation case (thin line), (d) excretion by zooplankton of the small case of –2‰, the control case of –5‰ and the large case of –8‰, (e) egestion by zooplankton of the small case of –0‰, the control case of –2‰ and the large case of –4‰ and (f) decompositions of the small case of –0‰, the control case of –1‰ and the large case of –2‰. Dashed, thick and dotted lines and open circles are small, control and large cases and observed values, respectively. Open circles and triangles indicate observed vales of sinking particles from August 1998 to August 1999 and from September 1999 to June 2000, respectively.

els are low in autumn bloom and winter, unlike the seasonal trends for the NPZD-A2 and control models (Fig. 8(d)). This is because phytoplankton in the NPZD model assimilates nitrate, which is poor in ^{15}N from autumn to winter. For the NPZD-A2 model, which added nitrification to the NPZD-A1 model, δ^{15}N values of ammonium, phytoplankton and sinking PON show the same trends as those from the control model.

As previously discussed, the generalized NPZD model can almost reproduce the seasonal variations in the observed fluxes of sinking PON. This model can also reproduce the observed minimum δ^{15}N values during the spring bloom. However, the model does not reproduce the observed δ^{15}N increase of sinking PON from autumn to winter. The NPZD-A2 and control models, which have ammonium assimilation and nitrification added to the generalized NPZD model, can reproduce the observed seasonal δ^{15}N values well. We conducted case studies in

comparison with observed data at high latitude, where ammonium accumulates in subsurface water from autumn to winter. Our model including assimilation and nitrification of ammonium simulates the seasonal variations in δ^{15}N of sinking PON at high latitude better than the generalized NPZD model.

4.2 Sensitivity studies of isotopic fractionation effects

The isotopic fractionation effect (ε (‰)) for each process is set to a mean value of the fractionation effects estimated in previous studies. To investigate the sensitivity of each isotopic fractionation effect to the seasonal δ^{15}N variations in our model, we conducted case studies varying each effect within a possible range and compared these results with the observed seasonal variations in δ^{15}N of sinking particles.

Figure 9(a) shows a comparison of the δ^{15}N of sinking particles among three experiments by changing the isotopic fractionation effect of nitrate assimilation by phytoplankton: 0‰ (non-fractionation case), –5‰ (control case) and –10‰ (large case). In the control and large cases (thick and dashed lines, respectively), the δ^{15}N of sinking particles in the spring bloom has its annual minimum, although that of the non-fractionation case (dotted line) does not. Figures 9(b) and (c) show comparisons of the δ^{15}N of sinking particles among experiments changing the isotopic fractionation effect of ammonium assimilation by phytoplankton: –5‰ (small case), –10‰ (control case) and –15‰ (large case) and the isotopic fractionation effect of nitrification: 0‰ (non-fractionation case), –9‰ (small case), –14‰ (control case) and –19‰ (large case), respectively. All cases of δ^{15}N of sinking particles show approximately the same values in spring, but different values from summer to winter. Only in the non-fractionation case does the δ^{15}N of sinking particles show extremely low values in winter (Fig. 9(c)). The annual maximum δ^{15}N of sinking particles in winter can be simulated with large isotopic fractionation of nitrification. Figures 9(d) and (e) display comparisons of the δ^{15}N of sinking particles from three experiments varying in isotopic fractionation effects of excretion by zooplankton: –2‰ (small case), –5‰ (control case) and –8‰ (large case) and the isotopic fractionation effect of egestion by zooplankton: 0‰ (non-fractionation case), –2‰ (control case) and –4‰ (large case), respectively. In all cases, the δ^{15}N of sinking particles show almost the same values from spring to summer, and slightly different values from summer to winter. Figure 9(f) shows a comparison of the δ^{15}N of sinking particles from three experiments varying in isotopic fractionation effects of both decomposition and remineralization: 0‰ (non-fractionation case), –1‰ (control case) and –2‰ (large case). In all three cases, the isotopic fractionations by decomposition and remineralization contribute little to the seasonal variations in δ^{15}N of sinking particles.

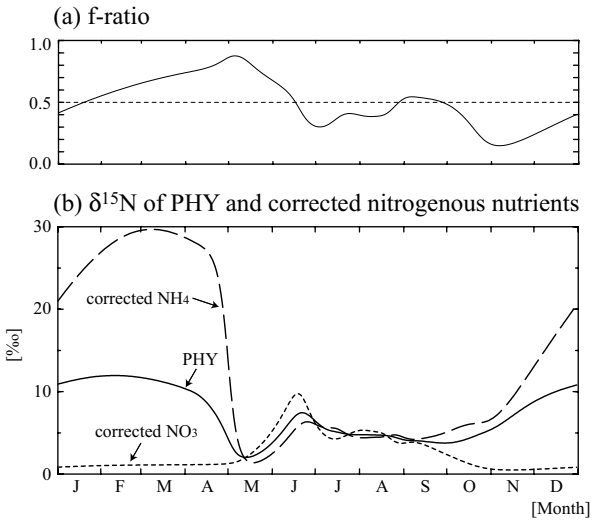

Fig. 10. Seasonal variations: (a) *f*-ratio and (b) the three kinds of δ^{15}N of phytoplankton in the upper later when allowed to assimilate 1. both nitrate and ammonium (solid line), 2. only nitrate (dotted line) and 3. only ammonium (dashed line). δ^{15}N values of phytoplankton assumed to assimilate only nitrate and ammonium are calculated using the isotopic fractionation effects of –10‰ and –5‰, respectively.

Three fractionations contributing most to δ^{15}N of sinking particles are those for nitrate and ammonium uptakes by phytoplankton and nitrification (Figs. 9(a), (b) and (c)). The minimum δ^{15}N in the spring bloom are affected only by fractionation from nitrate uptake, and the maximum δ^{15}N in winter are affected by all three fractionations. We need precise values of isotopic fractionation effects during nitrate and ammonium uptakes by phytoplankton, and nitrification is important to understanding seasonal δ^{15}N variations in the surface water.

5. Discussion

5.1 Seasonal variations in δ^{15}N of phytoplankton

Phytoplankton assimilates nitrate with isotopic fractionation, and thus there is an inverse relationship between δ^{15}N of nitrate and nitrate concentration. The δ^{15}N information of nitrate is transmitted to the δ^{15}N of phytoplankton. Therefore, δ^{15}N of suspended PON in surface water, which consist of mainly phytoplankton, have been used to understand the degree of nutrient utilization in previous studies (Altabet and McCarthy, 1985; Altabet *et al.*, 1991). In our model, δ^{15}N of phytoplankton is determined by the inflows to PHY (compartment of phytoplankton in Fig. 2), since there are no isotopic fractionations of the outflows. Figure 10(b) shows the

three kinds of simulated δ^{15}N values of phytoplankton, which assimilate both nitrate and ammonium, only nitrate, and only ammonium, respectively. δ^{15}N values of phytoplankton assumed to assimilate only nitrate and ammonium are calculated using the isotopic fractionation effects of –10‰ and –5‰ (see Table 3 and Fig. 10 caption), respectively. In the spring bloom, δ^{15}N values of assimilated nitrate (dotted line in Fig. 10(b)) are higher than those of assimilated ammonium (dashed line in Fig. 10(b)), because *f*-ratios show high values, that is, phytoplankton assimilate mainly nitrate with isotopic fractionation. In the autumn bloom, δ^{15}N values of assimilated ammonium are higher than those of assimilated nitrate, because low δ^{15}N of nitrate supply from the lower layer and *f*-ratios show low values, that is, phytoplankton assimilate mainly ammonium with isotopic fractionation. There is a maximum of about 5‰ difference in δ^{15}N values of phytoplankton between the spring and autumn blooms, which assimilates only nitrate, and only ammonium, respectively. We suggest that observations of δ^{15}N of phytoplankton, nitrate and ammonium in the spring and autumn blooms may indicate the ratios of nutrient selectivity by phytoplankton. In winter, δ^{15}N of assimilated ammonium show extremely high values of about 30‰. The δ^{15}N of PHY in winter is the highest at 13‰ in a year, because of the uptake of high δ^{15}N of ammonium assimilated with an *f*-ratio of 0.3–0.7, even though the δ^{15}N of nitrate is at its minimum.

To understand why ammonium in winter has extremely high δ^{15}N in this model, we consider the effects affecting the seasonal variation in δ^{15}N of ammonium. δ^{15}N of NH_4 (ammonium compartment in Fig. 2) is determined by both processes of ammonium production and consumption. Because the exchange of ammonium between the upper and lower layers is strong in winter due to convective mixing, we can consider the average ammonium concentration for those two boxes, ANH_4. In winter, the δ^{15}N of ANH_4 increases while its concentration decreases (Figs. 11(a) and (b)). The total budget of the ANH_4 in winter shows a deficit, meaning that ANH_4 decreases (Fig. 11(c)). Nitrification, which is one of the consumption processes of the ANH_4, is the largest sink for ANH_4 (Nitri in Fig. 11(c)). To show the effect of each production and consumption process on the δ^{15}N values of ANH_4, we define the δ^{15}N tendency of ANH_4 as follows:

$$\frac{F}{ANH_4}\left(\delta^{15}N_F - \delta^{15}N_{ANH_4}\right),$$

where F and $\delta^{15}N_F$ are the δ^{15}N and flux of each process, and ANH_4 and $\delta^{15}N_{ANH4}$ are the average δ^{15}N and its flux. The positive tendency of δ^{15}N of ANH_4 in winter is affected only by nitrification, because other inflows and outflows are much smaller than the flux of nitrification (Nitri in Fig. 11(c)). That is, δ^{15}N and concentrations of ammonium in winter increase and decrease, respectively, reflecting almost only nitrification. δ^{15}N of ammonium has not been observed in winter and the nitrogen cycle in winter is not yet understood in terms of the fate of ammonium. The observation may indicate the consumption ratio of ammonium in winter, which is accumulated by biological activity from summer to autumn. We consider

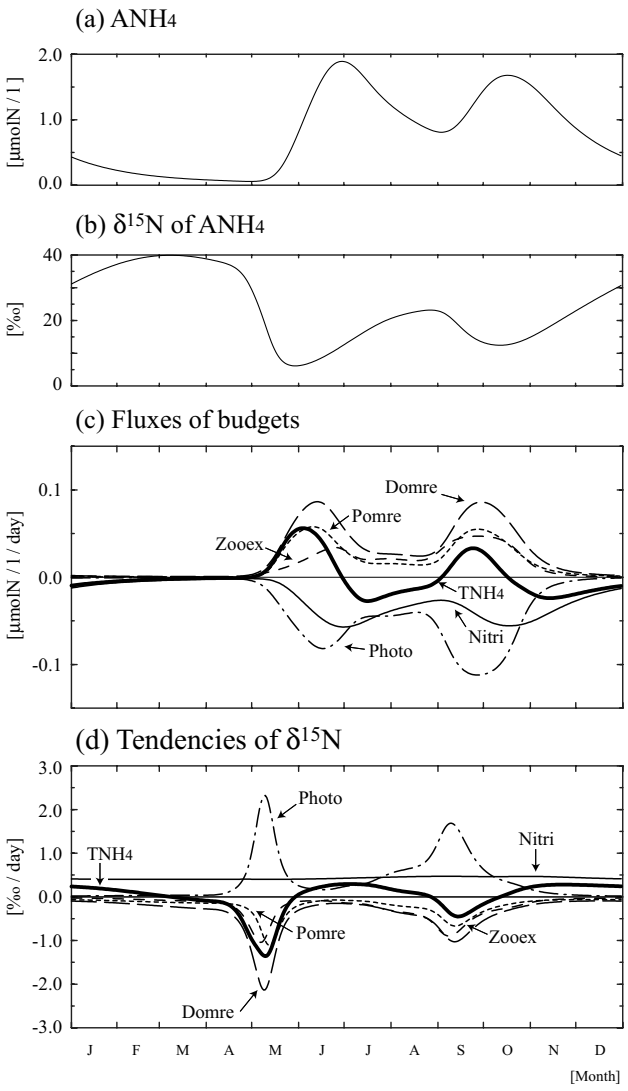

Fig. 11. Seasonal variations of (a) simulated ANH_4 concentration, which is the average of ammonium in the upper and lower layers, (b) simulated δ^{15}N values of ANH_4, (c) the fluxes of budgets of the ANH_4: average budget of ANH_4 (bold line), remineralization of PON (Pomre: dotted line), remineralization of DON (Domre: dashed line), excretion of zooplankton (Zooex: broken line), nitrification (Nitri: solid line) and photosynthesis (Photo: dash-dotted line), and (d) the tendencies of δ^{15}N values as defined in the text.

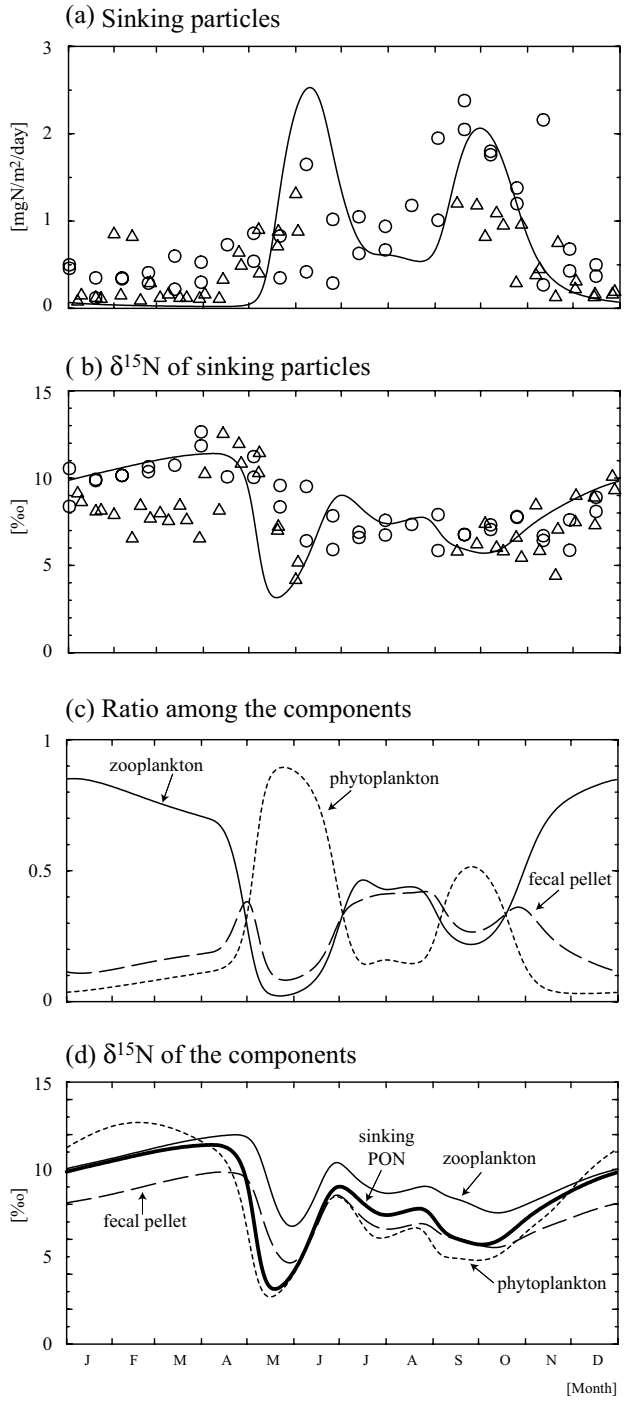

Fig. 12. Seasonal variations of (a) simulated (solid line) and observed (open circle: August 1998–August 1999, open triangle: September 1999–June 2000) fluxes of sinking particles, (b) simulated (solid line) and observed (open circle: August 1998–August 1999, open triangle: September 1999–June 2000) δ^{15}N values of sinking particles, (c) simulated ratio among components of sinking particles which originated from dead bodies of phytoplankton (phytoplankton: short-dashed line), dead bodies of zooplankton (zooplankton: solid line) and fecal pellet (fecal pellet: long-dashed line), in the sinking particles, and (d) simulated δ^{15}N values of dead bodies of phytoplankton (phytoplankton: short-dashed line), dead bodies of zooplankton (zooplankton: solid line), fecal pellet (fecal pellet: long-dashed line), and sinking particles (sinking PON: thick line). The values in (a) and (b) are the same as those in Figs. 4(f) and 5(e).

that the nitrification rate can be parameterized with observations of δ^{15}N of ammonium in winter and a sensitive study varying the parameter of nitrification rate.

5.2 *Seasonal variations in δ^{15}N of sinking particles*

δ^{15}N information of phytoplankton, which records the δ^{15}N information of nutrients, is further transmitted to δ^{15}N values of sinking particles. Thus, δ^{15}N values of sinking particles have been widely used to reproduce δ^{15}N information in nutrient conditions of surface water (Altabet and Deuser, 1985; Altabet *et al.*, 1991, 1999; Altabet and Francois, 1994, 2001; Voss *et al.*, 1996; Nakatsuka and Handa, 1997; Wu *et al.*, 1999; Peña *et al.*, 1999). We detailed the effect of seasonal variations in δ^{15}N values of sinking particles as follows. Figures 12(a) and (b) show the seasonal variations in flux and δ^{15}N of sinking PON in comparison with the sediment trap experiment at 300 m depth off East Sakhalin in the Sea of Okhotsk shown in Fig. 1. The sinking particles consist of dead bodies of phytoplankton and zooplankton and fecal pellets of zooplankton, in proportions that vary seasonally (Fig. 12(c)). The sinking particles are rich in phytoplankton during the spring bloom. The three components are present in roughly equal proportions from summer to autumn. During winter, approximately 90% of sinking particles are derived from zooplankton. The δ^{15}N of sinking particles is determined by the ratio among components of the PON and δ^{15}N of each component. Thus, the δ^{15}N of sinking particles approaches that of phytoplankton during the spring bloom and shows the mean value of the three components from summer to autumn, and it approaches the δ^{15}N of zooplankton in winter (Fig. 12(d)). The δ^{15}N of phytoplankton from spring to early autumn is 1‰ lower than that of fecal pellet and 3‰ lower than that of zooplankton, which is consistent with previous studies (Minagawa and Wada, 1984; Altabet and Small, 1990; Montoya *et al.*, 1990; Wu *et al.*, 1997; Adams and Sterner, 2000).

The δ^{15}N of each of the three components increases gradually from autumn to winter (Fig. 12(d)). Previous studies pointed out three reasons why δ^{15}N of sinking particles from autumn to winter increases despite the decrease in δ^{15}N of surface nitrate: (1) the contribution of zooplankton, which have a δ^{15}N about 3‰ higher than that of phytoplankton (Altabet *et al.*, 1991; Voss *et al.*, 1996; Peña *et al.*, 1999; Altabet and Francois, 2001); (2) the contribution of old particles most degraded with isotope fractionation in a year (Altabet *et al.*, 1991; Peña *et al.*, 1999; Altabet and Francois, 2001); and (3) the contribution of the most fractionated particles by trophic level transfer via the longest food web structure of the year during winter (Wu *et al.*, 1999; Peña *et al.*, 1999). We estimate from Fig. 12(d) that the first effect contributes about 40% and that the second contributes about 4% from spring to winter, but there is little contribution from autumn to winter (Fig. 7(f)). We found that the contribution of about 60% to the increased δ^{15}N of sinking particles was from the increase in δ^{15}N of ammonium and phytoplankton by nitrification. The third effect is not represented in our model. However, the samples of sinking particles in winter included various zooplanktons, which are both herbivorous and omnivorous zooplankton. δ^{15}N of omnivorous zooplankton is still higher than that of herbivorous zooplankton, especially in winter when trophic level becomes high (Wu *et al.*, 1999; Peña *et al.*, 1999). Therefore, the third effect may contribute to the increase in δ^{15}N of sinking particles in winter, and the estimation of the ratios of contributions about nitrification and contribution of zooplankton to the δ^{15}N of sinking particles in winter using our model may be somewhat overestimated. Models representing many classes of plankton explicitly should allow us to estimate the third effect. In this model, we would consider the effect of mineral ballasts (Klaas and Archer, 2002), although our model in this study does not consider this effect as it comprises only one class of planktons. The effect of mineral ballasts should also affect the δ^{15}N values of sinking particles in winter.

6. Summary

To clarify the potential of nitrogen isotopic studies for understanding the marine nitrogen cycles, we have developed an ecosystem model including nitrogen isotopes. Applied to the Sea of Okhotsk, this model successfully reproduced the concentrations of chlorophyll-a, ammonium and nitrate and the δ^{15}N of nitrate from observations over three seasons (spring, summer and autumn). It also reproduced the seasonal variations in the δ^{15}N and fluxes of sinking particles obtained from sediment trap experiments.

From the sensitivity studies changing isotopic fractionation effects, we found that the annual minimum δ^{15}N of sinking particles in the spring bloom is sensitive to the fractionation effect during nitrate assimilation by phytoplankton, but insensitive to other fractionation effects, and that the δ^{15}N increase of sinking particles from autumn to winter is sensitive to three fractionation effects of nitrification and nitrate and ammonium assimilations by phytoplankton. We also conducted case studies comparing the generalized four-compartment model with our six-compartment model. Both models could reproduce the observed δ^{15}N minimum of sinking PON during the spring bloom. However, from autumn to winter, the generalized model did not agree with the δ^{15}N increases of sinking PON from our six-compartment model and observation. A model that added ammonium assimilation and nitrification to the generalized model could represent the observed δ^{15}N increases from autumn to winter.

For simulations of seasonal variations in the δ^{15}N of sinking PON at high latitudes where ammonium accumulates in subsurface water, our model, which included ammonium assimilation and nitrification, is more suitable than the generalized model, which did not include these processes.

We detailed seasonal variations in δ^{15}N of phytoplankton. In our model, the δ^{15}N of phytoplankton are determined by δ^{15}N of nitrate and ammonium, and the *f*-ratio. In the spring and autumn blooms there was a difference between δ^{15}N values of phytoplankton, which assimilates only nitrate or ammonium. We suggest that observations of δ^{15}N of phytoplankton, nitrate and ammonium in the spring and autumn blooms can indicate the ratios of nutrient selectivity by phytoplankton. In winter, the δ^{15}N of phytoplankton is the highest in a year, because of the uptake of high δ^{15}N of ammonium with the *f*-ratio being from 0.3 to 0.7, even though the δ^{15}N of nitrate is at its minimum. δ^{15}N and concentrations of ammonium in winter, increase and decrease, respectively, reflecting almost only nitrification. We also suggest that the nitrification rate may be parameterized with observations of δ^{15}N of ammonium in winter and a sensitivity study varying the parameter of nitrification rate.

Nitrogen fixation and denitrification are important processes for considering nitrogen budget in the global ocean, although the values of the parameters for nitrogen fixation and denitrification in previous studies have great uncertainties. As there are many observations of these processes using δ^{15}N, nitrogen isotopes would help us to set the parameters for these processes. As a result, we could estimate the precise nitrogen budget in the global ocean.

Acknowledgements

We thank Prof. M. Wakatsuchi who coordinated this work as part of "Joint Japanese-Russian-U.S. Study of the Sea of Okhotsk". Special thanks are also due to Prof. K. Kawamura and Prof. E. Wada who discussed the work with us, to Dr. S. L. Smith and Mr. T. Ikeda who proofread the English manuscript, to Dr. G. Mizuta and Dr. Y. Fukamachi who offered the current velocity data, to Ms. M. N. Aita who provided us with her data interpolated from the NCEP data, and to Ms. M. Toda who supplied the chlorophyll-a data. Corresponding author, C. Yoshikawa, has benefited from financial support from Frontier Research Center for Global Change, JAMSTEC, to compile this work.

Appendix A. Equations in the Model

A.1. Governing equations for the nitrogen cycle

All equations for the nitrogen cycle are the same as those developed by KKYS. The prognostic variables are

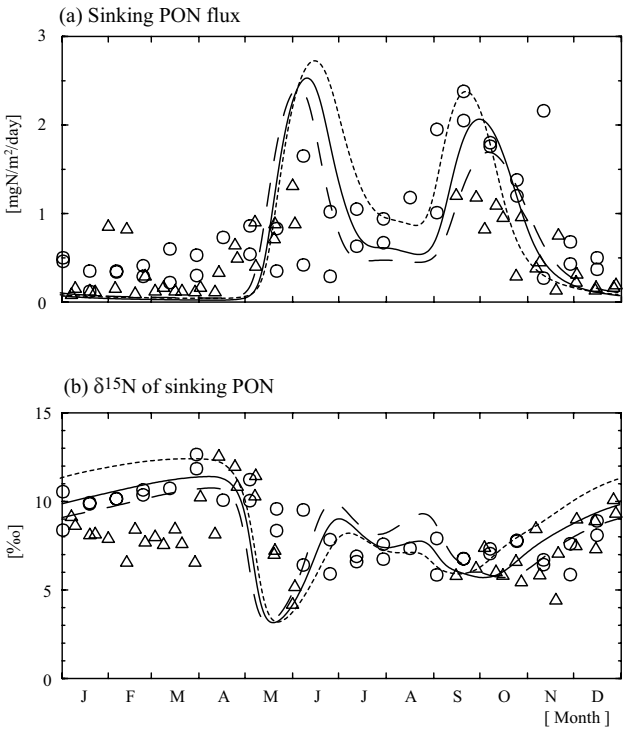

Fig. A1. Comparisons of fluxes (a) and δ^{15}N values (b) of sinking particles among experiments changing the coefficient of water exchange between the upper and lower layers (g_1) to half (dashed lines) and twice values (dotted lines). Open circles and triangles indicate observed vales of sinking particles from August 1998 to August 1999 and from September 1999 to June 2000, respectively.

PHY, ZOO, PON, DON, NO_3 and NH_4. The prognostic variables for nitrogen cycle are calculated as units of μmol/l, a function of time, and each box using the following six governing equations:

$$d[\mathrm{PHY}]/dt = (\mathrm{Photosynthesis}) - (\mathrm{Respiration}) - (\mathrm{Mortality}_{\mathrm{PHY}}) - (\mathrm{Grazing}) - (\mathrm{Extracellular\ Excretion}) + \mathrm{Exc(PHY)}, \quad \text{(A1)}$$

$$d[\mathrm{ZOO}]/dt = (\mathrm{Grazing}) - (\mathrm{Mortality}_{\mathrm{ZOO}}) - (\mathrm{Egestion}) - (\mathrm{Excretion}) + \mathrm{Exc(ZOO)}, \quad \text{(A2)}$$

$$d[\mathrm{NO_3}]/dt = -\{(\mathrm{Photosynthesis}) - (\mathrm{Respiration})\} \times F_{\mathrm{NEW}} + (\mathrm{Nitrification}) + \mathrm{Exc(NO_3)}, \quad \text{(A3)}$$

$$d[\mathrm{NH_4}]/dt = (\mathrm{Excretion}) + (\mathrm{Remineralization}_{\mathrm{PON}}) + (\mathrm{Remineralization}_{\mathrm{DON}}) - (\mathrm{Nitrification}) - \{(\mathrm{Photosynthesis}) - (\mathrm{Respiration})\} \times (1 - F_{\mathrm{NEW}}) + \mathrm{Exc(NH_4)}, \quad \text{(A4)}$$

$$d[\mathrm{PON}]/dt = (\mathrm{Mortality}_{\mathrm{PHY}}) + (\mathrm{Mortality}_{\mathrm{ZOO}}) + (\mathrm{Egestion}) - (\mathrm{Remineralization}_{\mathrm{PON}}) - (\mathrm{Decomposition}) - (\mathrm{Sinking}) + \mathrm{Exc(PON)}, \quad \text{(A5)}$$

$$d[\mathrm{DON}]/dt = (\mathrm{Decomposition}) + (\mathrm{Extracellular\ Excretion}) - (\mathrm{Remineralization}_{\mathrm{DON}}) + \mathrm{Exc(DON)}, \quad \text{(A6)}$$

where terms representing each process are described below.

Exc(C) represents the vertical exchange process between upper and lower layers for a specific compartment, C. That is, Exc(C) is defined as follows:

$$\mathrm{Exc}(C_{\mathrm{upper}}) = -\mathrm{Exc}(C_{\mathrm{lower}}) = -1/g_1(C_{\mathrm{upper}} - C_{\mathrm{lower}}). \quad \text{(A7)}$$

For NO_3 in the lower layer, nitrate supply from the deeper layer is also included.

$$\mathrm{Exc}([\mathrm{NO_3}]_{\mathrm{lower}}) = -1/g_1([\mathrm{NO_3}]_{\mathrm{upper}} - [\mathrm{NO_3}]_{\mathrm{lower}}) - 1/g_2([\mathrm{NO_3}]_{\mathrm{lower}} - [\mathrm{NO_3}]_{\mathrm{deeper}}), \quad \text{(A8)}$$

where g_1 and g_2 are the coefficients of vertical exchange (Fig. 3). g_1 cannot be constrained by the observed data, as this coefficient is given in reference to the observed vertical distribution of monthly temperature. We conducted a sensitivity study changing g_1 to half and double values, since mixed layer depths should greatly affect the surface biological activities in high latitude (Fig. A1). In the small exchange case, the peak in spring bloom and the drop timing in δ^{15}N are earlier than those in the control case. This is due to early improvement of light condition by the stratification. In the large exchange case, the peak in autumn bloom is earlier than those in the control case. This is due to early nitrate supply by the convective mixing. In spite of changing g_1 to half and double values, the shifts of peaks in the spring and autumn blooms and of δ^{15}N drop in the spring bloom are within 2 weeks in these cases, and the seasonal variations in fluxes and δ^{15}N values are common characteristics in these cases. We conclude that the uncertainty of g_1 does not affect the discussion in this study. The coefficient of g_2 is set to a typical value below the bottom of the mixed layer. We confirmed that g_2 is insensitive to seasonal variations in prognostic values.

Photosynthesis by phytoplankton is formulated as follows:

$$(\mathrm{Photosynthesis}) = V_{\max}\left\{\frac{[\mathrm{NO_3}]}{[\mathrm{NO_3}]+K_{\mathrm{NO_3}}}\exp(-\Psi[\mathrm{NH_4}]) + \frac{[\mathrm{NH_4}]}{[\mathrm{NH_4}]+K_{\mathrm{NH_4}}}\right\} \cdot \exp(kT) I_{\mathrm{photo}}[\mathrm{PHY}], \quad \text{(A9)}$$

where I_{photo} is light intensity in the each layer, and T is temperature (Fig. 3). For calculating the vertical average of I_{photo} using the following vertical integration, we divide each layer into sublayers of 1 m, respectively.

$$I_{\mathrm{photo}} = \frac{\int_0^z \left(\frac{I(z)}{I_{\mathrm{opt}}}\exp\left(1-\frac{I(z)}{I_{\mathrm{opt}}}\right)\right)dz}{\int_0^z dz}, \quad \text{(A10)}$$

$$I(z) = I_{\mathrm{surface}}\exp\left\{-\left(a_1 + a_2[\mathrm{PHY}]_{\mathrm{upper}}\right)z\right\} \quad \text{for the upper layer,} \quad \text{(A11)}$$

$$I(z) = I_{(20\mathrm{m})}\exp\left\{-\left(a_1 + a_2[\mathrm{PHY}]_{\mathrm{lower}}\right)(z-20\mathrm{m})\right\} \quad \text{for the lower layer,} \quad \text{(A12)}$$

where I_{surface} is light intensity at the sea surface (Fig. 3) and z is the depth of sublayers. The f-ratio can be defined as

$$F_{\mathrm{new}} = \frac{\frac{[\mathrm{NO_3}]}{[\mathrm{NO_3}]+K_{\mathrm{NO_3}}}\exp(-\Psi[\mathrm{NH_4}])}{\frac{[\mathrm{NO_3}]}{[\mathrm{NO_3}]+K_{\mathrm{NO_3}}}\exp(-\Psi[\mathrm{NH_4}]) + \frac{[\mathrm{NH_4}]}{[\mathrm{NH_4}]+K_{\mathrm{NH_4}}}}. \quad \text{(A13)}$$

Respiration, extracellular excretion, mortality, grazing and egestion of plankton types are represented as follows:

$$(\mathrm{Respiration}) = V_{\mathrm{p0}}\exp(k_{\mathrm{R}}T)[\mathrm{PHY}], \quad \text{(A14)}$$

$$(\mathrm{Extracellular\ excretion}) = \gamma(\mathrm{Photosynthesis}), \quad \text{(A15)}$$

$$(\mathrm{Mortality}_{\mathrm{PHY}}) = M_{\mathrm{P0}}\exp(k_{\mathrm{MP}}T)[\mathrm{PHY}]^2, \quad \text{(A16)}$$

$$(\mathrm{Mortality}_{\mathrm{ZOO}}) = M_{\mathrm{Z0}}\exp(k_{\mathrm{MZ}}T)[\mathrm{ZOO}]^2, \quad \text{(A17)}$$

$$= G_{R\max}\max\left[0, 1-\exp\left\{\lambda_{\mathrm{S}}\left(P_Z^* - [\mathrm{PHY}]\right)\right\}\exp(k_{\mathrm{GS}}T)[\mathrm{ZOO}]\right], \quad \text{(A18)}$$

$$(\mathrm{Excretion}) = (\alpha - \beta)(\mathrm{Grazing}), \quad \text{(A19)}$$

$$(\text{Egestion}) = (1-\alpha)(\text{Grazing}). \quad \text{(A20)}$$

Remineralization of PON, DON, decomposition and nitrification are represented as follows:

$$(\text{Remineralization}_{\text{PON}}) = V_{\text{PA0}} \exp(k_{\text{PA}} T)[\text{PON}], \quad \text{(A21)}$$

$$(\text{Remineralization}_{\text{DON}}) = V_{\text{DA0}} \exp(k_{\text{DA}} T)[\text{DON}], \quad \text{(A22)}$$

$$(\text{Decomposition}_{\text{DON to DON}}) = V_{\text{PD0}} \exp(k_{\text{PD}} T)[\text{PON}], \quad \text{(A23)}$$

$$(\text{Nitrification}) = N_{\text{Nit0}} \exp(k_{\text{Nit}} T)[\text{NH}_4]. \quad \text{(A24)}$$

Sinking of particles is described by:

$$(\text{Sinking}_{\text{PON}}) = \frac{1}{\Delta Z}(S_{\text{PON}}[\text{PON}]), \quad \text{(A25)}$$

where ΔZ is the thickness of upper (20 m) and lower (100 m) layers. Values of parameters described in this subsection are shown in Table 3.

A.2. Governing equations for the ^{15}N cycle

All equations for the ^{15}N cycle are based on the above equations for the nitrogen cycle. The prognostic variables for the ^{15}N cycle are calculated as a function of time, t, and each box using the following six governing equations:

$$\begin{aligned} &d[^{15}\text{N}_{\text{PHY}}]/dt \\ &= \{(\text{Photosynthesis}) - (\text{Respiration})\} \times F_{\text{NEW}} \times R_{\text{NO}_3} \times \alpha_1 \\ &\quad + \{(\text{Photosynthesis}) - (\text{Respiration})\} \times (1 - F_{\text{NEW}}) \times R_{\text{NH}_4} \\ &\quad \times \alpha_2 - (\text{Mortality}_{\text{PHY}}) \times R_{\text{PHY}} - (\text{Grazing}) \times R_{\text{PHY}} \\ &\quad - (\text{Extracellular Excretion}) \times R_{\text{PHY}} + \text{Exi(PHY)}, \end{aligned} \quad \text{(A26)}$$

$$\begin{aligned} &d[^{15}\text{N}_{\text{ZOO}}]/dt \\ &= (\text{Grazing}) \times R_{\text{PHY}} - (\text{Mortality}_{\text{ZOO}}) \times R_{\text{ZOO}} \\ &\quad - (\text{Egestion}) \times R_{\text{ZOO}} \times \alpha_3 \\ &\quad - (\text{Excretion}) \times R_{\text{ZOO}} \times \alpha_4 + \text{Exi(ZOO)}, \end{aligned} \quad \text{(A27)}$$

$$\begin{aligned} &d[^{15}\text{NO}_3]/dt \\ &= -\{(\text{Photosynthesis}) - (\text{Respiration})\} \times F_{\text{NEW}} \times R_{\text{NO}_3} \times \alpha_1 \\ &\quad + (\text{Nitrification}) \times R_{\text{NH}_4} \times \alpha_5 + \text{Exi}(\text{NO}_3), \end{aligned} \quad \text{(A28)}$$

$$\begin{aligned} &d[^{15}\text{NH}_4]/dt \\ &= (\text{Excretion}) \times R_{\text{ZOO}} \times \alpha_4 \\ &\quad + (\text{Remineralization}_{\text{PON}}) \times R_{\text{PON}} \times \alpha_6 \\ &\quad + (\text{Remineralization}_{\text{DON}}) \times R_{\text{DON}} \times \alpha_7 \\ &\quad - (\text{Nitrification}) \times R_{\text{NH}_4} \times \alpha_5 \\ &\quad - \{(\text{Photosynthesis}) - (\text{Respiration})\} \times (1 - F_{\text{NEW}}) \times R_{\text{NH}_4} \\ &\quad \times \alpha_2 + \text{Exi}(\text{NH}_4), \end{aligned} \quad \text{(A29)}$$

$$\begin{aligned} &d[\text{PO}^{15}\text{N}]/dt \\ &= (\text{Mortality}_{\text{PHY}}) \times R_{\text{PHY}} + (\text{Mortality}_{\text{ZOO}}) \times R_{\text{ZOO}} \\ &\quad + (\text{Egestion}) \times R_{\text{ZOO}} \times \alpha_3 \\ &\quad - (\text{Remineralization}_{\text{POM}}) \times R_{\text{PON}} \times \alpha_6 \\ &\quad - (\text{Decomposition}) \times R_{\text{PON}} \times \alpha_8 - (\text{Sinking}) \times R_{\text{PON}} \\ &\quad + \text{Exi(PON)}, \end{aligned} \quad \text{(A30)}$$

$$\begin{aligned} &d[\text{DO}^{15}\text{N}]/dt \\ &= (\text{Decomposition}) \times R_{\text{PON}} \times \alpha_8 \\ &\quad + (\text{Extracellular Excretion}) \times R_{\text{PHY}} \\ &\quad - (\text{Remineralization}_{\text{DON}}) \times R_{\text{DON}} \text{¥} \, a_7 + \text{Exi(DON)}, \end{aligned} \quad \text{(A31)}$$

where R_C are ratios of ^{15}N/N for a specific compartment, C, and α_l are isotopic fractionation coefficient. That is, α_l are calculated by:

$$\alpha_l = \exp(\varepsilon_l/1000) \quad \text{(A32)}$$

where ε_l are isotopic fractionation effects listed in Table 3.

Also, Exi(C) represent the vertical exchange process for ^{15}N cycle between upper and lower layers for a specific compartment, C, defined as follows:

$$\begin{aligned} &\text{Exi}(C_{\text{upper}}) \\ &= -\text{Exi}(C_{\text{lower}}) = -1/g_1\left(C_{\text{upper}} \times R_{C_{\text{upper}}} - C_{\text{lower}} \times R_{C_{\text{lower}}}\right). \end{aligned} \quad \text{(A33)}$$

For $^{15}NO_3$ in the lower layer, the ^{15}N of nitrate supply from the deeper layer is also included.

$$\begin{aligned}
&\mathrm{Exi}\left(\left[{}^{15}\mathrm{NO_3}\right]_{\mathrm{lower}}\right)\\
&= -1/g_1\\
&\quad\cdot\left(\left[{}^{15}\mathrm{NO_3}\right]_{\mathrm{upper}} \times R_{\mathrm{NO_3\ upper}} - \left[{}^{15}\mathrm{NO_3}\right]_{\mathrm{lower}} \times R_{\mathrm{NO_3\ lower}}\right)\\
&\quad -1/g_2\\
&\quad\cdot\left(\left[{}^{15}\mathrm{NO_3}\right]_{\mathrm{lower}} \times R_{\mathrm{NO_3\ lower}} - \left[{}^{15}\mathrm{NO_3}\right]_{\mathrm{deeper}} \times R_{\mathrm{NO_3\ deeper}}\right),
\end{aligned} \tag{A34}$$

where g_1 and g_2 are the coefficients of vertical exchange (Fig. 3).

The δ^{15}N values for a specific compartment C are calculated by:

$$\begin{aligned}
&\delta^{15}\mathrm{N}(‰)\\
&= \left[\frac{\left\{\left[{}^{15}\mathrm{N}\right]/\left([\mathrm{N}]-\left[{}^{15}\mathrm{N}\right]\right)\right\}_{\mathrm{of}\ C}}{\left\{\left[{}^{15}\mathrm{N}\right]/\left([\mathrm{N}]-\left[{}^{15}\mathrm{N}\right]\right)\right\}_{\mathrm{of\ Atmospheric\ N_2}}} - 1\right] \times 1000,
\end{aligned} \tag{A35}$$

where Atmospheric N_2 is defined as a standard sample including [^{15}N] being 0.365%.

References

Adams, T. A. and R. W. Sterner (2000): The effect of dietary nitrogen content on trophic level ^{15}N enrichment. *Limnol. Oceanogr.*, **45**, 601–607.

Altabet, M. A. and W. G. Deuser (1985): Seasonal variations in natural abundance of ^{15}N in particles sinking to the deep Sargasso Sea. *Nature*, **315**, 218–219.

Altabet, M. A. and R. Francois (1994): Sedimentary nitrogen isotopic ratio as a recorder for surface ocean nitrate utilization. *Global Biogeochem. Cycles*, **8**, 103–116.

Altabet, M. A. and R. Francois (2001): Nitrogen isotope biogeochemistry of the Antarctic Polar Frontal Zone at 170°W. *Deep-Sea Res. II*, **48**, 4247–4273.

Altabet, M. A. and J. J. McCarthy (1985): Temporal and spatial variations in the natural abundance of ^{15}N in PON from a warm-core ring. *Deep-Sea Res.*, **32**, 755–772.

Altabet, M. A. and L. F. Small (1990): Nitrogen isotope ratios in fecal pellets produced by marine zooplankton. *Geochim. Cosmochim. Acta*, **54**, 155–163.

Altabet, M. A., W. G. Deuser, S. Honjo and C. Stienen (1991): Seasonal and depth-related changes in the source of sinking particles in the North Atlantic. *Nature*, **354**, 136–138.

Altabet, M. A., C. Pilskaln, C. P. Thunell, D. Sigman, F. Chavez and R. Francois (1999): The nitrogen isotope biogeochemistry of sinking particles from the margin of the Eastern North Pacific. *Deep-Sea Res. I*, **46**, 655–679.

Casciotti, K. L., D. M. Sigman and B. B. Ward (2003): Linking diversity and stable isotope fractionation in ammonium-oxidizing bacteria. *Geomicrobiology J.*, **20**, 335–353.

Checkley, D. M. and C. A. Miller (1989): Nitrogen isotope fractionation by oceanic zooplankton. *Deep-Sea Res.*, **36**, 1449–1456.

Cifuentes, L. A., M. L. Fogel, J. R. Pennock and J. H. Sharp (1989): Biogeochemical factors that influence the stable nitrogen isotope ratio of dissolved ammonium in the Delaware Estuary. *Geochim. Cosmochim. Acta*, **53**, 2713–2721.

David, R. (2001): δ^{15}N as an integrator of the nitrogen cycles. *Trends in Ecology & Evolution*, **16**, 153–162.

Dugdale, R. C. and F. P. Wilkerson (1986): The use of ^{15}N to measure nitrogen uptake in eutrophic oceans; experimental considerations. *Limnol. Oceanogr.*, **31**, 673–689.

Fujii, M., Y. Nojiri, Y. Yamanaka and M. J. Kishi (2002): A one-dimensional ecosystem model applied to time series Station KNOT. *Deep-Sea Res. II*, **49**, 5441–5461.

Giraud, X., P. Bertrand, V. Garçon and I. Dadou (2000): Modeling δ^{15}N evolution: First palaeoceanographic applications in a coastal upwelling system. *J. Mar. Res.*, **58**, 609–630.

Giraud, X., P. Bertrand, V. Garçon and I. Dadou (2003): Interpretation of the nitrogen isotopic signal variations in the Mauritanian upwelling with a 2D physical-biogeochemical model. *Global Biogeochem. Cycles*, **17**, 2801–2819.

Hoch, M. P., R. A. Snyder, L. A. Cifuentes and R. B. Coffin (1996): Stable isotope dynamics of nitrogen recycled during interactions among marine bacteria and protests. *Mar. Ecol. Prog. Ser.*, **132**, 229–239.

Honda, M. C., M. Kusakabe, S. Nakabayashi, S. J. Manganini and S. Honjo (1997): Change in pCO_2 through biological activity in the marginal sea of the Western North Pacific: the efficiency of the biological pump estimated by a sediment trap experiment. *J. Oceanogr.*, **53**, 645–662.

Horrigan, S. G., J. P. Montoya, J. L. Nevins and J. J. McCarthy (1990): Natural isotopic composition of dissolved inorganic nitrogen in the Chesapeake Bay. *Estuar., Coast. Shelf Sci.*, **30**, 393–410.

Imai, K., Y. Nojiri, N. Tsurushima and T. Saino (2002): Time series of seasonal variation of primary productivity at station KNOT (44°N, 155°E) in the sub-arctic western North Pacific. *Deep-Sea Res. II*, **49**, 5395–5408.

Kawamiya, M., M. J. Kishi, Y. Yamanaka and N. Suginohara (1997): Procuring reasonable results in different oceanic regimes with the same ecological-physical coupled model. *J. Oceanogr.*, **53**, 397–402.

Klaas, C. and D. E. Archer (2002): Association of sinking organic matter with various types of mineral ballast in the deep sea: Implications for the rain ratio. *Global Biogeochem. Cycles*, **16**, doi:10.1029/2001GB001765.

Minagawa, M. and E. Wada (1984): Stepwise enrichment of ^{15}N along food chains: Further evidence and the relation between δ^{15}N and animal age. *Geochim. Cosmochim. Acta*, **48**, 1135–1140.

Miyake, Y. and E. Wada (1971): The isotope effect on the nitrogen in biochemical, oxidation—Reduction reactions. *Records of Oceanographic Works in Japan*, **11**, 1–6.

Mizuta, G., Y. Fukamachi, K. I. Ohshima and M. Wakatsuchi (2003): Structure and seasonal variability of the East Sakhalin Current. *J. Phys. Oceanogr.*, **33**, 2430–2445.

Montoya J. P. and J. J. McCarthy (1995): Isotopic fractionation during nitrate uptake by phytoplankton grown in continuous culture. *J. Plankton Res.*, **17**, 439–464.

Montoya, J. P., S. G. Horrigan and J. J. McCarthy (1990): Natural abundance of ^{15}N in particulate nitrogen and zooplankton in the Chesapeake Bay. *Mar. Ecol. Prog. Ser.*, **65**, 35–61.

Montoya, J. P., S. G. Horrigan and J. J. McCarthy (1991): Rapid, storm-induced changes in the natural abundance of ^{15}N in a planktonic ecosystem, Chesapeake Bay, USA. *Geochim. Cosmochim. Acta*, **55**, 3627–3638.

Nakatsuka, T. and N. Handa (1997): Reconstruction of seasonal variation in nutrient budget of a surface mixed layer using $\delta^{15}N$ of sinking particle collected by a time-series sediment trap system. *J. Oceanogr.*, **53**, 105–116.

Nakatsuka, T., T. Fujimune, C. Yoshikawa, S. Noriki, K. Kawamura, Y. Fukamachi, G. Mizuta and M. Wakatsuchi (2004): Biogenic and lithogenic particle fluxes in the western region of the Sea of Okhotsk: implications for lateral material transport and biological productivity. *J. Geophys. Res.*, **109**, C09S13, doi:10.1029/2003JC001908.

Ohshima, K. I., M. Wakatsuchi, Y. Fukamachi and G. Mizuta (2002): Near-surface circulation and tidal currents of the Okhotsk Sea observed with the satellite-tracked drifters. *J. Geophys. Res.*, **107**, 3195, doi:10.1029/2001JC001005.

Oschlies, A. and V. Garçon (1999): An eddy-permitting coupled physical-biological model of the North Atlantic. *Global Biogeochem. Cycles*, **13**, 135–160.

Ostrom, N. E., S. A. Macko, D. Deibel and R. J. Thompson (1997): Seasonal variation in the stable carbon and nitrogen isotope biogeochemistry of a coastal cold ocean environment. *Geochim. Cosmochim. Acta*, **61**, 2929–2942.

Peña, M. A., K. L. Denman, S. E. Calvert, R. E. Thomson and J. R. Forbes (1999): The seasonal cycle in sinking particle fluxes off Vancouver Island, British Columbia. *Deep-Sea Res. II*, **46**, 2969–2992.

Pennock, J. R., D. J. Velinsky, J. M. Ludlam and M. L. Fogel (1996): Isotopic fractionation of ammonium and nitrate during uptake by *Skeletonema costatum*: Implications for $\delta^{15}N$ dynamics under bloom conditions. *Limnol. Oceanogr.*, **41**, 451–459.

Saino, T. and A. Hattori (1980): ^{15}N natural abundance in oceanic suspended particulate matter. *Nature*, **283**, 752–754.

Saino, T. and A. Hattori (1987): Geographical variation of the water column distribution of suspended particulate organic nitrogen and its ^{15}N natural abundance in the Pacific and its marginal seas. *Deep-Sea Res.*, **34**, 807–827.

Sambrotto, R. N. (2001): Nitrogen production in the northern Arabian Sea during the Spring Intermonsoon and Southwest Monsoon seasons. *Deep-Sea Res. II*, **48**, 1173–1198.

Sambrotto, R. N. and B. J. Mace (2000): Coupling of biological and physical regimes across the Antarctic Polar Front as reflected by nitrogen production and recycling. *Deep-Sea Res. II*, **47**, 3339–3367.

Sigman, D. M., M. A. Altabet, D. C. McCorkle, R. Francois and G. Fischer (1999): The $\delta^{15}N$ of nitrate in the Southern Ocean: Consumption of nitrate in surface waters. *Global Biogeochem. Cycles*, **13**, 1149–1166.

Sorokin, Y. I. and P. Y. Sorokin (1999): Production in the Sea of Okhotsk. *J. Plankton Res.*, **21**, 201–230.

Sutka, R. L., N. E. Ostrom, P. H. Ostrom and M. S. Phanikumar (2004): Stable nitrogen isotope dynamics of dissolved nitrate in a transect from the North Pacific Subtropical Gyre to the Eastern Tropical North Pacific. *Geochem. Cosmochim. Acta*, **68**, 517–527.

Voss, M., M. A. Altabet and B. V. Bodungen (1996): $\delta^{15}N$ in sedimenting particles as indicator of euphotic-zone processes. *Deep-Sea Res. I*, **43**, 33–47.

Wada, E. (1980): Nitrogen isotope fractionation and its significance in biogeochemical processes occurring in marine environments. p. 375–398. In *Isotope Marine Chemistry*, ed. by E. D. Goldberg and Y. Horibe, Uchida Rokakuho, Tokyo.

Waniek, J. J. (2003): The role of physical forcing in initiation of spring blooms in the northeast Atlantic. *J. Mar. Sys.*, **39**, 57–82.

Waser, N. A., K. Yin, Z. Yu, K. Tada, P. J. Harrison, D. H. Turpin and S. E. Calvert (1998): Nitrogen isotope fractionation during nitrate, ammonium and urea uptake by marine diatoms and coccolithophores under various conditions of N availability. *Mar. Ecol. Prog. Ser.*, **169**, 29–41.

Wilkerson, F. P., R. C. Dugdale, R. M. Kudela and F. P. Chavez (2000): Biomass and productivity in Monterey Bay, California: contribution of the large phytoplankton. *Deep-Sea Res. II*, **47**, 1003–1022.

Wu, J., S. E. Calvert and C. S. Wong (1997): Nitrogen isotope variations in the subarctic northeast Pacific: relationships to nitrate utilization and trophic structure. *Deep-Sea Res. I*, **44**, 287–314.

Wu, J., S. E. Calvert, C. S. Wong and F. A. Whitney (1999): Carbon and nitrogen isotopic composition of sedimenting particulate material at Station Papa in the subarctic northeast Pacific. *Deep-Sea Res. II*, **46**, 2793–2832.

Yamanaka, Y., N. Yoshie, M. Fujii, M. N. Aita and M. J. Kishi (2004): An ecosystem model coupled with Nitrogen-Silicon-Carbon cycles applied to Station A7 in the Northwestern Pacific. *J. Oceanogr.*, **60**, 227–241.

Yoshikawa, C., T. Nakatsuka, K. Kawamura and M. Wakatsuchi (2001): Seasonal changes in the fluxes of total organic carbon and the $\delta^{15}N$ of the sinking particles off the east coast of Sakhaline Island. p. 106–107. In *Proceedings of the International Symposium on Atmosphere-Ocean-Cryosphere Interaction in the Sea of Okhotsk and the Surrounding Environment*, ed. by M. Wakatsuchi and T. Hara.

Yoshikawa, C., T. Nakatsuka, K. Kawamura and M. Wakatsuchi (2005): The $\delta^{15}N$ of nitrate and N* as the tracers for the nitrogen cycle in the Sea of Okhotsk (in preparation).